ADAPTIVE ESTIMATION OF LI-ION BATTERY MODEL PARAMETERS

by

Daniyal Ali

A Thesis Presented to the Faculty of the
American University of Sharjah
College of Engineering
in Partial Fulfillment
of the Requirements
for the Degree of

Master of Science in
Electrical Engineering

Sharjah, United Arab Emirates

May 2016

Approval Signatures

We, the undersigned, approve the Master's Thesis of Daniyal Ali.

Thesis Title: Adaptive Estimation of Li-ion Battery Model Parameters.

Signature	**Date of Signature** (dd/mm/yyyy)
_____	_____
Dr. Shayok Mukhopadhyay Assistant Professor, Department of Electrical Engineering Thesis Advisor	
_____	_____
Dr. Habib-ur Rehman Associate Professor, Department of Electrical Engineering Thesis Co-advisor	
_____	_____
Dr. Rached Bin H'mida Dhaouadi Professor, Department of Electrical Engineering Thesis Committee Member	
_____	_____
Dr. Jin-Hyuk Lee Assistant Professor, Department of Mechanical Engineering Thesis Committee Member	
_____	_____
Dr. Nasser Qaddoumi Head, Department of Electrical Engineering	
_____	_____
Dr. Mohamed El-Tarhuni Associate Dean, College of Engineering	
_____	_____
Dr. Leland Blank Dean, College of Engineering	
_____	_____
Dr. Khaled Assaleh Interim Vice Provost for Research and Graduate Studies	

Acknowledgements

First of all I would like to thank Almighty Allah for blessing me with this opportunity to do my Master's thesis. I would like to thank my parents who always supported me and believed in me at every step of my life.

I want to pay my gratitude to my advisors Dr. Shayok Mukhopadhyay and Dr. Habib-ur Rehman who contributed with their valuable guidance and support to complete this thesis. They dedicated their time and it was due to their tireless efforts that I have reached my destination. I would specially like to thank Dr. Habib-ur Rehman for informing me about this assistantship opportunity and who has been always helpful throughout my stay here at the American University of Sharjah (AUS).

My thanks go to the faculty of engineering and the college of electrical engineering for providing me with a platform along with the graduate student assistantship that made it possible for me to achieve this milestone.

Also, a special thanks to my teammate and friend Adil Khurram who did not spare an effort in supporting and assisting me in my journey. Lastly, I would like to thank my family and friends who made this journey enjoyable and unforgettable.

Dedicated to you as a reader . . .

Abstract

This work presents a novel application of a high gain adaptive observer-based technique for Lithium-ion (Li-ion) battery modeling. The model used in this work was originally developed by Chen and Mora. However, in Chen and Mora's original work, the parameters required for the battery model were estimated through intensive experimentation. In contrast, this work presents an adaptive observer for estimating the battery model parameters. This results in the reduction of experimental effort required to estimate battery model parameters. The selected model (Chen and Mora's model) requires twenty one parameters to accurately model a Li-ion battery. This work initially proposes three variations of a high gain adaptive observer-based technique to adaptively tune fifteen of the required parameters accurately. The remaining six parameters related to the shape of the no-load electromotive-force (EMF) curve are obtained via a voltage relaxation test. Based on observations made during simulations of the above proposed techniques, an improved estimation technique is proposed in the latter half of this document, and experimental results validating the proposed technique are presented. Experiments show that the model obtained through this technique is independent of the magnitude and type of load. The improved parameter estimation technique is justified using rigorous mathematical analysis. The proposed improved technique can be used either online or offline for estimating battery model parameters. This may be valuable for automatically updating battery models parameters on-board future smart vehicles in real time.

Search Terms: ***Adaptive Parameter Estimation, Li-ion Battery, Universal Adaptive Stabilization***

Table of Contents

List of Figures

List of Tables

Chapter 1: Introduction and Literature Review

Lithium-ion batteries have become an attractive choice because of their ability to handle numerous charge/discharge cycles and their good power to weight ratio. Also, problems like the recovery effect are not prominent in Li-ion batteries. On average, a Li-ion battery can store up to one hundred and fifty watt-hours of energy per kilogram [1]. An accurate state of charge (SOC) estimation of a Li-ion battery is important because it can be used to ascertain the capacity left in the battery. If a battery is discharged completely (i.e., its SOC $= 0$), then adverse effects are observed upon the next charge/discharge cycle. The SOC of a given battery cannot be measured directly, but needs to be estimated [2]. Unless computationally expensive estimation strategies like particle filtering [3] are used, the precision of SOC estimation depends upon the accuracy of the battery model opted. Some challenges related to Li-ion battery modeling, state estimation, and control are summarized in [4]. An overview and a comparison of state of charge estimation methods for Li-ion batteries is presented in [5].

Battery modeling has been extensively investigated in the literature. An overview of different types of battery models is presented in [6]. Moreover, six different type of Li-ion battery models are discussed in [7] and state estimation techniques are also presented. The model discussed in [8] is an electro-chemical model, which is mainly used to relate design parameters to battery voltage and current for optimizing the physical design features of batteries. Electrochemical models are complex because they are usually modeled by partial differential equations, whose solution requires a lot of computational effort. A mathematical model used to predict the residual energy of a battery is discussed in [9]. Most of the mathematical models do not provide essential information related to the dynamics of a battery such as current and voltage, which are essential for any accurate circuit simulation. The mathematical model presented in [10] is developed specifically for a pocket computer; hence, it is application specific.

An equivalent circuit model of a battery is more attractive because it can provide real-time voltage and current dynamics under varying loads. Furthermore, it is easy to integrate the effects of battery parameters variation in such models because they do not lead to a substantial increase in the computational effort required to solve

the model equations. The equivalent circuit models are further divided into three major categories: namely run-time models, impedance-based models and Thevenin-based models [11]. The model provided in [12] encapsulates nonlinear equilibrium potentials, rate and temperature dependencies, thermal effects, and response to transient power demand. Chen and Mora's model [11] is also an equivalent circuit model, which is used in this work. Chen and Mora's model is selected because it captures the essential dynamic characteristics i.e. nonlinear open-circuit voltage, current, temperature, cycle number, storage time-dependent capacity and transient response of a battery, and the effects of load current changes. Effects related to cycle number, temperature, and storage time dependent capacity loss may also be captured via this model by relating these effects to the SOC. This makes the model [11] versatile, and therefore provides further motivation to use it in this work.

Extracting all parameters of any given battery model is usually a time consuming process because multiple iterations of an experiment need to be performed for accurate parameter estimation. Adaptive algorithms can be used to reduce the experimental effort required for battery modeling. Examples of work needing a lot of experimentation are found in [11] and [13]. In [14], [15] and [16] the moving window least squares method is used to estimate parameters. The observer gains in [15] are selected using the linear quadratic (LQ) approach, and in [16] the observer gains are selected using the pole placement method. A Lyapunov-based approach is used in [17] for online parameters estimation. This method only uses the battery voltage and current measurements to estimate battery parameters. A non-linear least squares method from [3] is used in [18] to estimate battery model parameters, and the model in [18] is able to handle noise corrupted input and output data. A curve-fitting-based method is proposed in [13]. In [19], a Thevenin-based model is used along with an adaptive extended Kalman Filter (AEKF) to estimate the SOC. Different SOC estimation methods are also discussed in [19] and the AEKF approach is verified to be more accurate compared to other discussed approaches. The experimental results are used as a reference to compute the accuracy. In [20], an equivalent circuit-based model is proposed, and a multi-objective optimization technique is used to extract the model parameters. A linear parameter varying battery model is proposed in [21], and model identification is done using battery voltage

and current measurements. The cell-to-cell variability of capacity and internal resistance of a Li-ion pack are discussed in [22] using a statistical modeling approach. The model in [22] allows verification of known relations between certain parameters (e.g., the capacity and internal resistance) of a battery. This helps in studying the variability and the effect of the above mentioned parameters on the entire battery pack. The authors in [23] present a way to predict the steady state characteristics of Li-ion battery using the data sheet provided by the manufacturer. In [24], the impedance in z-domain is used to estimate the Li-ion battery parameters, using a resistor to express the voltage drop in frequency domain.

The state of charge estimation and health of a battery-pack on a cellular level is presented in [25] using a model-driven approach that involves Kalman filtering and a Battery Monitoring System. An experimental method is discussed in [26], where the battery is discharged at different rates and interpolation of the data is done to obtain accurate model parameters. A PSPICE parametric model is presented in [27], with the aim of transferring parameter estimation techniques to PSPICE while working at the component level. An experimentally validated SOC estimator is used in [28] to estimate the capacity of a battery. In [29], methods like support vector machines and low-current Hybrid Pulse Power characterization (L-HPPC) are used to predict the state of charge and state of health of the battery. The standard least squares regression method is used in [30] to separately estimate the slow and fast dynamics of the battery. This leads to a better frequency response with a simple model. A non-chemical based partially linearized input-output battery model is proposed in [31]. The recovery effect is incorporated in this model [31] to increase the accuracy of the battery lifetime estimation. Artificial Neural Networks (ANN) are used in [32] to estimate the remaining battery capacity. State and parameter estimation of an electrochemical model of a battery using a multi-rate particle filer is proposed in [33]. The voltage data is divided into several thresholds in [34] and a linear model is established at each threshold which helps in identifying the parameters of the battery easily. State of charge estimation based on an adaptive nonlinear observer design is presented in [35]. While different load profiles are plotted to validate the accuracy of the obtained estimation. In [36], a thermal model

is used to estimate the inner temperature of a Li-ion battery. The relation of battery capacity and temperature is also analyzed using the model obtained.

The aim of this work is to develop a modeling methodology that reduces the time spent on gathering experimental data for battery modeling. Another aim is to develop a method which can be used either online or offline and to enable battery model identification for future applications without requiring any substantial downtime. Such online identification schemes allow for better performance, even if the battery degrades over time. Therefore, a high gain adaptive observer-based methodology for modeling Li-ion batteries is proposed. The adaptive observer is utilized to estimate the battery model parameters, so that the difference between the output terminal voltage obtained from a model and the terminal voltage of a real battery is minimized. This work shows a novel use of a high-gain adaptive strategy for battery modeling. This research is inspired by earlier work in [37], where a high gain adaptive observer is used to detect abrupt changes in the battery states, which detects an impending battery terminal voltage collapse. To make the model more accurate, three schemes based on the above mentioned adaptive methodology are initially tested and verified through intensive computer simulations.

The first scheme can only estimate large valued parameters. The second scheme can estimate all parameters with reasonable accuracy. However, both the first and second schemes are more dependent upon the proper choices of the model parameters' initial conditions. In contrast, the third scheme can estimate all the parameters of Chen and Mora's battery model, even if rough estimates of the bounds on the initial conditions for the parameters are known, though the initial conditions still need to be close to the original parameters values.

Based on the observations and analysis of the above mentioned three techniques, an improved estimation technique is presented. In this methodology, curve fitting is used to estimate the parameters of the open circuit voltage curve, and the battery series resistance. The remaining parameters are estimated using a classical high-gain adaptive technique. The advantage of this technique is that battery parameters can be estimated with sufficient accuracy within few experimental runs. It is shown that accuracy in SOC estimation is not sacrificed even if estimates of battery parameters do not converge to

their actual values. Further, it is proved that if the battery discharge current magnitude is sufficiently small, then the product of the estimated values of resistances and capacitances appearing in parallel branches in the equivalent circuit model, converges to the product of actual values of resistances and capacitances. If bounds on battery parameter values are known, which is practically possible, it is shown that accuracy of the estimated parameter values is improved. Above claims are supported by mathematical proofs and experimental results which show that battery parameters estimated using a constant load current are successfully able to model battery terminal voltage and provide sufficiently accurate SOC estimates even in the presence of variable load current.

1.1. Motivation

This work proposes a novel methodology using high-gain adaptive control theory for estimating parameters required for Chen and Mora's model. The proposed approach has advantages over other methods available in the literature. For example, using the least squares estimation method given in [14], [15] and [16] could result in computationally intensive algorithms as large matrices may need to be inverted. Similarly, the curve fitting method [13] to extract all battery parameters requires a lot of experimentation to get the required curves. Curve fitting also requires a suitable analytical form of an equation relating a particular parameter to a measured quantity. The approach used in this work doesn't require linearization of the battery model, unlike Kalman filter-based approaches [38]. The methodology suggested in this thesis uses an adaptive observer, which estimates model parameters which are valid independent of load current. It is observed that the model parameters' convergence obtained using the proposed observer is fast even in the presence of load changes, disturbances and battery nonlinearities. Thus, the observed speed of parameter convergence and non-dependence of model parameter estimates on load current are salient features of the developed method. Curve-fitting is used for estimating parameters of the output equation. However, this doesn't require extensive experimentation as only a no-load test is needed. The functional form for the output equation is also available from [11].

In the future, Li-S batteries might supersede Li-ion batteries. In [39], a literature review is done on different models used for the modeling the performance of Li-S batteries. This shows that the research on modeling of Li-ion batteries is moving one step further because now the modeling techniques on Li-S batteries are being researched and compared.

1.2. Thesis Organization

In chapter two, a brief background about the basic concepts of adaptive estimation and battery modeling is provided. Chapter three illustrates the concept of universal adaptive stabilization technique for a Li-ion battery. Then, chapter four provides implementation of the proposed battery parameters estimation methodology in simulations and mathematical validation is also presented. In chapter five, intensive experimentation is shown to validate the estimated battery parameters. Chapter six gives comparative analysis and limitations of the proposed methodology. In Chapter seven future works are discussed. Finally, chapter eight sums up the conclusion of the thesis.

Chapter 2: Background

2.1. Chen and Mora's Model

Chen Mora's model [11] used in this work is shown in Figure 1. The left half of the circuitry shown in Figure 1 models the battery state of charge dynamics. For this work, the self discharge resistance is neglected because the effects of battery self-discharge can be easily accounted for by multiplying the battery SOC by a certain factor f, where $0 < f < 1$. The right half of the circuitry shown in Figure 1 models the battery output voltage dynamics in response to changing load currents. The state x_1 represents the battery SOC, the state x_2 represents the voltage across $R_{ts}||C_{ts}$, and the state x_3 represents the voltage across $R_{tl}||C_{tl}$. The parallel combination $R_{ts}||C_{ts}$ models the short-term terminal voltage dynamics in response to changes in the discharge current. Similarly, the parallel combination $R_{tl}||C_{tl}$ models the long-term terminal voltage dynamics in response to changes in the discharge current. The state x_1 is normalized and can vary from [0,1], and the states $x_2, x_3 \in \mathbb{R}$. The state space equations for Chen and Mora's model as derived in [40] are:

$$\dot{x}_1(t) = -\frac{1}{C_c} i(t) \tag{2.1}$$

$$\dot{x}_2(t) = -\frac{x_2(t)}{R_{ts}(x_1)C_{ts}(x_1)} + \frac{i(t)}{C_{ts}(x_1)} \tag{2.2}$$

$$\dot{x}_3(t) = -\frac{x_3(t)}{R_{tl}(x_1)C_{tl}(x_1)} + \frac{i(t)}{C_{tl}(x_1)} \tag{2.3}$$

$$y = E_o(x_1) - x_2(t) - x_3(t) - i(t)R_s(x_1) \tag{2.4}$$

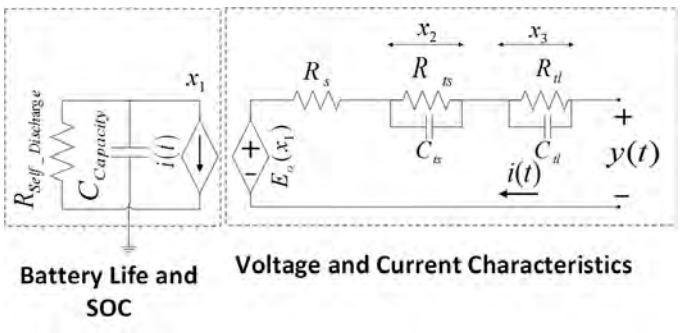

Figure 1: Chen and Mora's battery model

where the components R_{ts}, R_{tl}, C_{ts}, C_{tl}, R_s and E_o are given as follows:

$$R_{ts}(x_1) = a_1 e^{-a_2 x_1} + a_3 \tag{2.5}$$

$$R_{tl}(x_1) = a_4 e^{-a_5 x_1} + a_6 \tag{2.6}$$

$$C_{ts}(x_1) = -a_7 e^{-a_8 x_1} + a_9 \tag{2.7}$$

$$C_{tl}(x_1) = -a_{10} e^{-a_{11} x_1} + a_{12} \tag{2.8}$$

$$R_s(x_1) = a_{13} e^{-a_{14} x_1} + a_{15} \tag{2.9}$$

$$E_o(x_1) = -a_{16} e^{-a_{17} x_1} + a_{18} + a_{19} x_1 - a_{20} x_1^2 + a_{21} x_1^3. \tag{2.10}$$

R_s, R_{ts}, R_{tl}, C_{ts} and C_{tl} represent the various resistances and capacitances shown in Figure 1. The quantity E_o represents the open circuit EMF of a Li-ion battery, where $E_o : [0,1] \to [b_1, b_2]$ and $b_1, b_2 \in \mathbb{R}$, and $b_2 > b_1 \geq 0$. The parameters $a_i > 0$ for $i = \{1,2,3....21\}$ are the battery model parameters that need identification. Usually experimental procedures are undertaken in the literature to find a_1 to a_{21}. In this work, three schemes are initially tested. They are based on a high gain adaptive observer to estimate parameters a_1 to a_{15}, while a_{16} to a_{21} are easily obtainable via the voltage relaxation method [41]. Finally an improved adaptive parameters estimation scheme is presented along with all the necessary mathematical details.

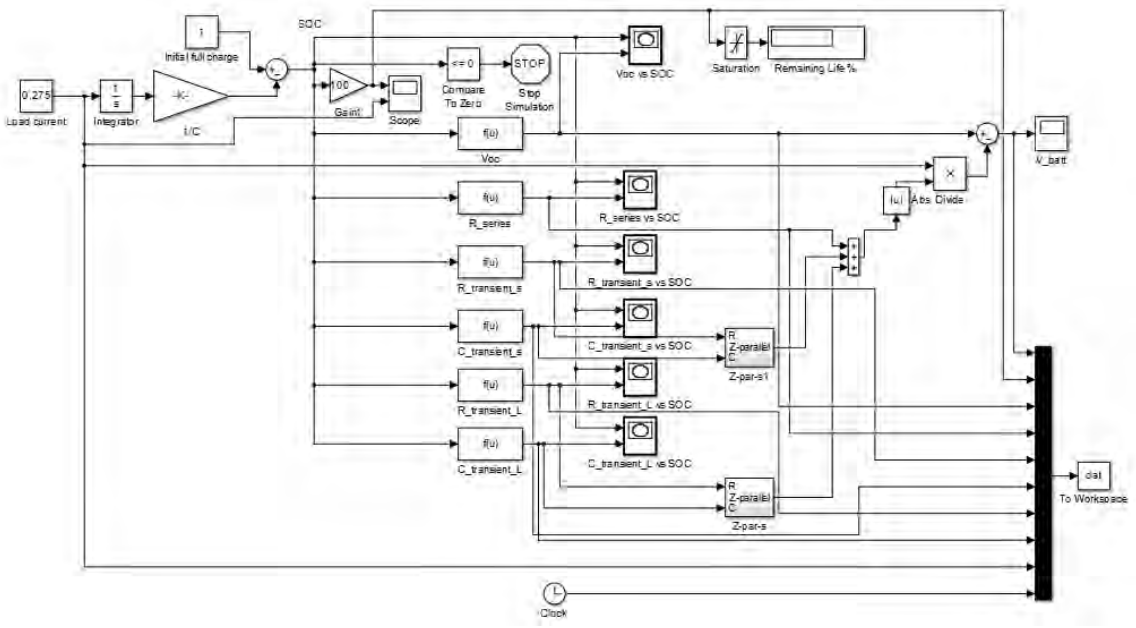

Figure 2: Simulation block diagram for Chen and Mora's model

2.1.1. Simulation of Chen and Mora's model. The Simulink block diagram shown in Figure 2 consists of different blocks corresponding to the model parameters (resistors, capacitors) shown in Figure 1. The plot of each component (R_s, R_{ts}, C_{ts}, R_{tl} and C_{tl}) is shown with respect to the state of charge in Figures 4, 5, 6, 7 and 8 respectively. Figure 3 shows the open circuit voltage (VOC) versus the state of charge (SOC) of the battery. The voltage curve is almost linear when the state of charge is higher, but becomes nonlinear once the state of charge decreases.

The behavior of R_s with respect to SOC is shown in Figure 4. It can be observed that the value of R_s changes drastically when the SOC of a Li-ion battery goes below 10%.

2.1.2. Battery stability conditions. The battery system represented by equations (2.1) - (2.4), looses stability when the battery terminal voltage drops suddenly [42]. Defining the equations for δ_1 and δ_2 as follows:

$$\delta_1 = -\frac{1}{a_8} \ln\left(\frac{a_9}{a_7}\right) \tag{2.11}$$

$$\delta_2 = -\frac{1}{a_{11}} \ln\left(\frac{a_{12}}{a_{10}}\right) \tag{2.12}$$

where, δ_1 and δ_2 provide the worst case limit for the state of charge of a battery. If the state of charge goes below δ_1 or δ_2, the battery must be switched off as the output voltage will soon experience sudden drop, making the battery system unstable. Note

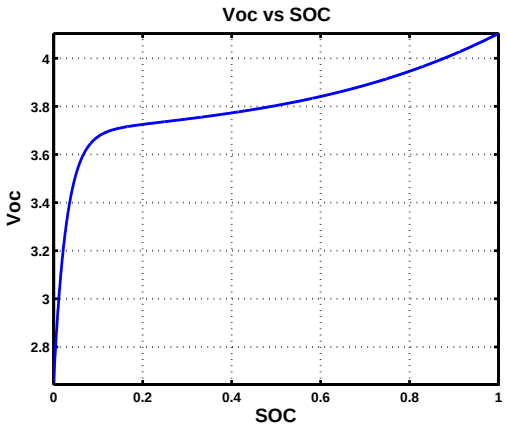

Figure 3: Open circuit voltage (VOC) vs state of charge (SOC)

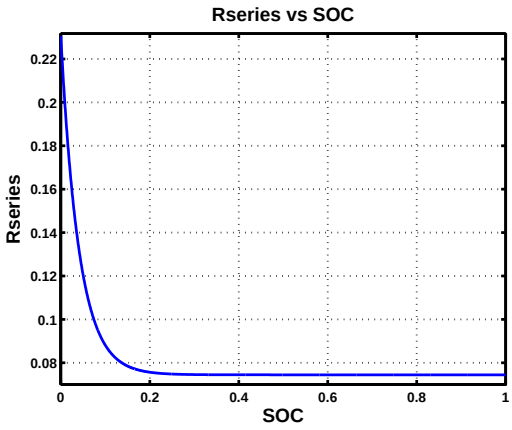

Figure 4: Series resistance of the battery (R_s) vs state of charge (x_1)

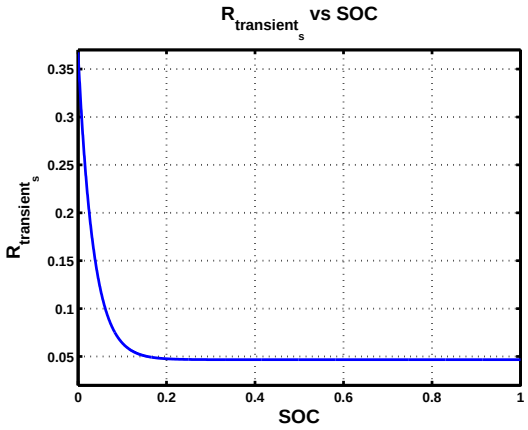

Figure 5: R_{ts} vs state of charge (x_1)

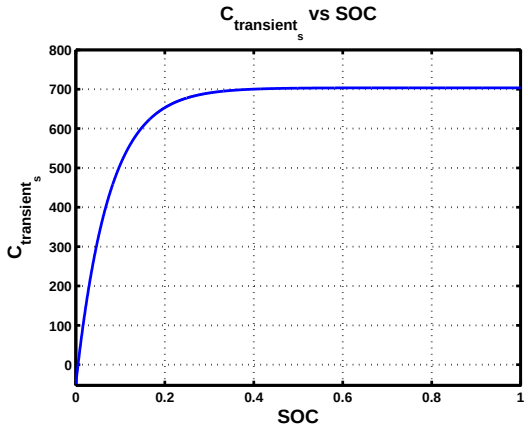

Figure 6: C_{ts} vs state of charge (x_1)

that more detailed proofs regarding the stability analysis of the model are discussed in [42].

2.2. Universal Adaptive Stablization (UAS)

A feedback control algorithm is usually used to achieve certain closed loop control objectives, for a known plant. The basic motivation for using adaptive control algorithms is that the plant is not always accurately known. The goal of UAS is to achieve control objectives using only the available structural information of a plant. The controller adjusts its parameters by estimating plant parameters from the output data of the plant. An overview of the universal adaptive stabilization approaches used in nonlinear control is given in [43]. A method for designing a universal adaptive sta-

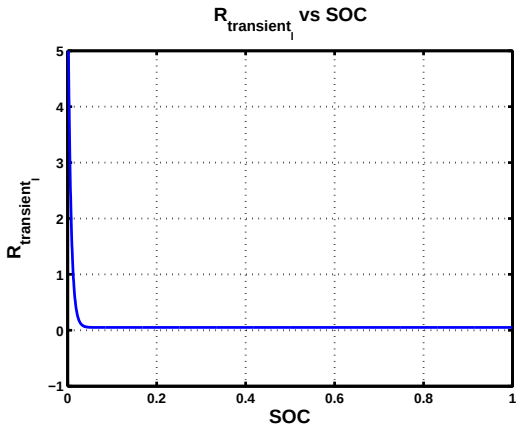

Figure 7: R_{tl} vs state of charge (x_1)

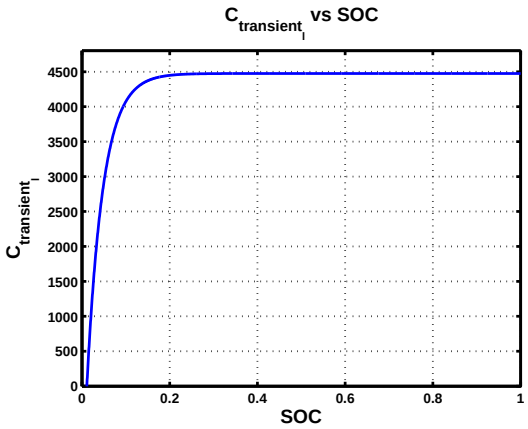

Figure 8: C_{tl} vs state of charge (x_1)

bilizer is presented in [44]. The work of Nussbaum and other researchers in the area of non-identifier based adaptive control [45] is the inspiration for our work.

2.2.1. Mittag-Leffler function. The Mittag-Leffler function is a special and complex function used for solutions of fractional equations [46]. It depends upon two parameters α and β. It is defined in equation (2.13). The series converges for all values of z whereas α and β are positive and real. We use the Mittag-Leffler function for tuning adaptive gain, and the details are presented later.

$$E_{\alpha,\beta}(z) = \sum_{k=0}^{\infty} \frac{z^k}{\Gamma(\alpha k + \beta)} \tag{2.13}$$

2.2.2. Nussbaum function. Universal Adaptive Stabilizers (UAS) often use Nussbaum functions [45]. Nussbaum functions are defined as below:

Definition 2.2.2.1: Let $k' \in R$. Piecewise right continuous functions are switching functions which allow identification of the sign of required control input. A piecewise right continuous function $N(\cdot) : [k', \infty) \to \mathbb{R}$ is called a Nussbaum function if it satisfies

$$\sup_{k>k_0} \frac{1}{k-k_0} \int_{k_0}^{k} N(\tau) d\tau = +\infty$$

and

$$\inf_{k>k_0} \frac{1}{k-k_0} \int_{k_0}^{k} N(\tau) d\tau = -\infty$$

for some $k_0 \in (k', \infty)$

Some examples of Nussbaum function extracted from [45] are shown below:

$$N_1(k) = k^2 cosk$$
$$N_2(k) = k(cos\sqrt{|k|})$$
$$N_3(k) = lnk(cos\sqrt{ln(k)})$$

2.2.3. Mittag-Leffler as Nussbaum function. A new family of Nussbaum functions has been found in [47] which can be expressed by Mittag Leffler functions

under certain conditions. The SIMULINK block diagram is obtained from [48] to simulate a Mittag Leffler function as a Nussbaum function. Figure 9 shows the simulink diagram of the implementation. The output plot of the simulation is shown in Figure 10. The Nussbaum function used for this work is further explained in Section 3.1 and more details are presented in [47].

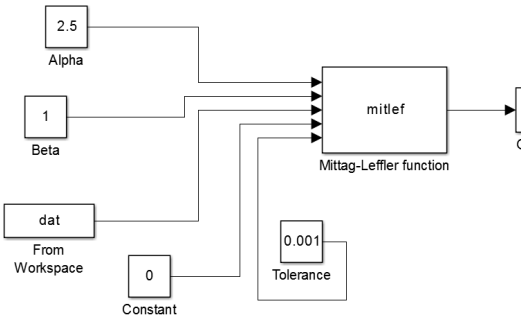

Figure 9: Mittag-Leffler as a Nussbaum function - block diagram

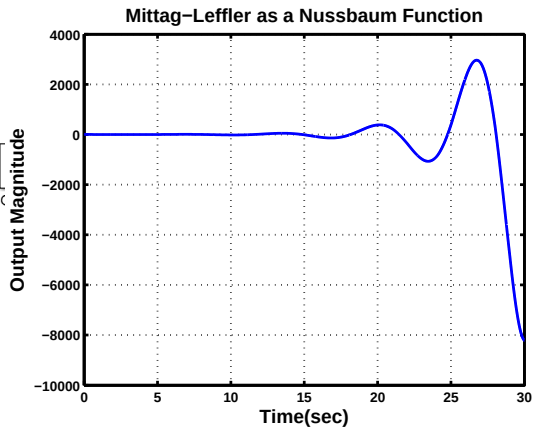

Figure 10: Mittag-Leffler as a Nussbaum function - output

Chapter 3: Adaptive Parameter Estimation for Li-ion Batteries

In this section, three candidate methods for identification of Li-ion battery parameters are presented. They are subsequently evaluated by rigorous simulation. This process helps in developing the final adaptive parameter estimation algorithm. The proposed methods consist of two steps; the first step being a voltage relaxation test for obtaining the shape of a no-load EMF curve which gives parameters $\widehat{a}_{16}$ to $\widehat{a}_{21}$ in equation (2.10). These parameters are determined by using the curve-fitting toolbox in MATLAB along with the no-load EMF curve obtained from the voltage relaxation test. Curve-fitting is used to obtain the parameters of the no-load EMF equation because no dynamics are available for it, thus rendering the use of any sort of dynamic parameter estimation scheme impractical. The second step of the proposed modeling methodology involves adaptive parameter estimation for parameters in the battery model state equations. For this, three possible schemes are provided. Details are presented in Sections 3.2.1, 3.2.2 and 3.2.3. The following steps present the outline for the proposed modeling methodology:

1. Perform voltage relaxation test to obtain no-load EMF curve for a given Li-ion battery.
2. Find parameters $\widehat{a}_{16}$ to $\widehat{a}_{21}$ for equation (2.10) by curve-fitting of the data obtained in step 3.
3. Select one of the three adaptive model parameter estimation schemes from Sections 3.2.1, 3.2.2 and 3.2.3.
4. Discharge the given Li-ion battery with any given load profile and store the measured terminal voltage and discharge current data.
5. Perform adaptive model parameter estimation for $\widehat{a}_1$ to $\widehat{a}_{15}$ using the data obtained from step 4, based upon a selected scheme in step 3.
6. If the error $e(t)$ in equation (3.15) converges to zero, then pick model parameters $\widehat{a}_1$ to $\widehat{a}_{15}$ as specified in Section 3.2.4.

3.1. Li-ion Battery Parameter Estimation - Overall Architecture

Figure 11 shows the overall architecture of the proposed battery parameter estimation technique. It consists of seven blocks. The left most block represents the load. The next block represents a physical (real) Li-ion battery. The current $i(t)$ is the actual current which the battery supplies to an external load. The Coulomb counting block takes this current $i(t)$ and provides the SOC by integration. The output voltage of the battery is represented by $y(t)$. The main block is the parameter estimation block. This block requires the SOC and the error $e(t) = y(t) - \widehat{y}(t)$. This block estimates the parameters a_1 to a_{15} in equations (2.5) to (2.9) by using one of the three schemes in equations (3.16), (3.17) or (3.18). The quantity $\widehat{y}(t)$ represents the terminal voltage output from the battery model in equations (3.2), (3.3) and (3.14). The battery model is shown by a dotted box in Figure 11. It contains two individual blocks; the dynamic equations block which represents the internal states of the battery model (equations (3.2) - (3.3)), and the model output voltage block which represents the output voltage given by equation (3.14).

The main idea of this work is to compute the control signal $u(t)$, and to simultaneously tune parameters $\widehat{a}_1$ to $\widehat{a}_{15}$ so that the error $e(t) \to 0$ as time goes to infinity, independent of the load current $i(t)$ being supplied by the real battery. For this purpose the universal adaptive stabilizer block is used, which is shown in Figure 11. This block continuously tunes parameters $\widehat{a}_1$ to $\widehat{a}_{15}$ so that the required objective, stated above can be met. It is hypothesized that, if the error $e(t)$ given by equation (3.15) converges to a sufficiently small value, then parameters $\widehat{a}_1$ to $\widehat{a}_{15}$ will have converged to certain values. It is further hypothesized that if a control signal $u(t)$ in Figure 11 can be picked so that the error $e(t)$ remains close to zero for a sufficiently long period of time, parameters a_{16} to a_{21} are known, and the initial guesses of $\widehat{a}_1$ to $\widehat{a}_{15}$ are reasonably close to their actual values, then $\widehat{a}_1$ to $\widehat{a}_{15}$ will converge to values which will provide the necessary model parameters for producing a reasonably accurate battery model independent of the load current. Before presenting the schemes for adaptive estimation of model parameters,

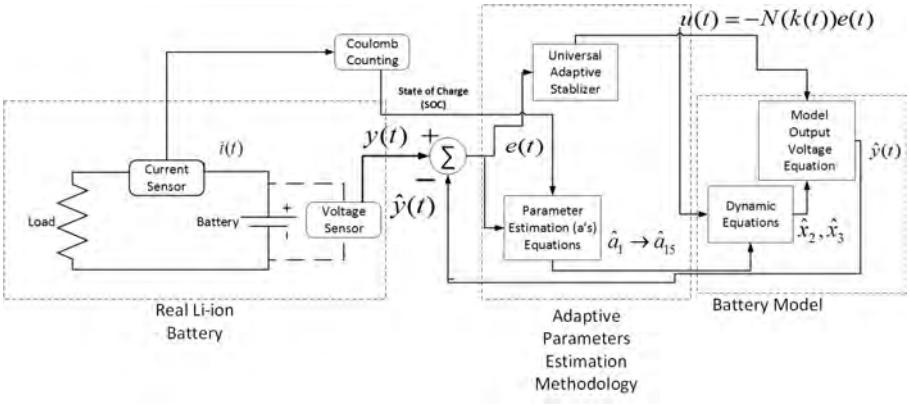

Figure 11: Li-ion battery parameter estimation algorithm - overall architecture

the battery model dynamic equations are proposed as follows:

$$\dot{\widehat{x}}_1 = \frac{-1}{Cc} i(t) \tag{3.1}$$

$$\dot{\widehat{x}}_2(t) = -\frac{\widehat{x}_2(t)}{\widehat{R}_{ts}(\widehat{x}_1)\widehat{C}_{ts}(\widehat{x}_1)} + u(t) \tag{3.2}$$

$$\dot{\widehat{x}}_3(t) = -\frac{\widehat{x}_3(t)}{\widehat{R}_{tl}(\widehat{x}_1)\widehat{C}_{tl}(\widehat{x}_1)} + u(t) \tag{3.3}$$

In the model equations, there are three states $\dot{\widehat{x}}_1$, $\dot{\widehat{x}}_2$ and $\dot{\widehat{x}}_3$. Moreover, we can measure current, and we are trying to estimate model parameters, so we are assuming that the coulomb counting definition, shown in equation (3.1) gives a good enough estimate of SOC, and even if there exist errors due to this, we show experimentally that this does not affect the model accuracy. It is also assumed that the structure of a battery model is known; hence equations (3.2) and (3.3) have similar analytical forms to Chen and Mora's model equations (i.e., equations (2.2) and (2.3)). Similarly, the circuit elements $\widehat{R}_{tl}$, $\widehat{C}_{tl}$, $\widehat{R}_{ts}$, $\widehat{C}_{ts}$ have the same analytical forms as to Chen and Mora's equations (i.e., equations (2.5) - (2.10))

$$\widehat{R}_{ts}(\widehat{x}_1) = \widehat{a}_1 e^{-\widehat{a}_2 \widehat{x}_1} + \widehat{a}_3 \tag{3.4}$$

$$\widehat{R}_{tl}(\widehat{x}_1) = \widehat{a}_4 e^{-\widehat{a}_5 \widehat{x}_1} + \widehat{a}_6 \tag{3.5}$$

$$\widehat{C}_{ts}(\widehat{x}_1) = -\widehat{a}_7 e^{-\widehat{a}_8 \widehat{x}_1} + \widehat{a}_9 \tag{3.6}$$

$$\widehat{C}_{tl}(\widehat{x}_1) = -\widehat{a}_{10}e^{-\widehat{a}_{11}\widehat{x}_1} + \widehat{a}_{12} \tag{3.7}$$

$$\widehat{R}_s(\widehat{x}_1) = \widehat{a}_{13}e^{-\widehat{a}_{14}\widehat{x}_1} + \widehat{a}_{15} \tag{3.8}$$

$$\widehat{E}_o(\widehat{x}_1) = -\widehat{a}_{16}e^{-\widehat{a}_{17}\widehat{x}_1} + \widehat{a}_{18} + \widehat{a}_{19}\widehat{x}_1 - \widehat{a}_{20}\widehat{x}_1^2 + \widehat{a}_{21}\widehat{x}_1^3. \tag{3.9}$$

The following equations are used to obtain $u(t)$ so that the adaptive observer can achieve $e(t) \to 0$ as time goes to infinity. In equation (3.12), $N(\cdot)$ represents a Nussbaum type switching gain [45], where $N(k(t))$ is defined as follows:

$$N(k(t)) = E_\alpha(\lambda k(t)^\alpha), \;\; \lambda > 0, \;\; \alpha \in (2,3) \tag{3.10}$$

where $E_\alpha(\cdot)$ is the Mittag-Leffler function [47, 49] defined below:

$$E_\alpha(z) = \sum_{k=0}^{\infty} \frac{z^k}{\Gamma(\alpha k + 1)} \tag{3.11}$$

Here $\Gamma(\cdot)$ represents the standard Gamma function (i.e., $\Gamma(z+1) = z\Gamma z, z > 0$) and α is a parameter.

$$u(t) = -N(k(t))e(t) \tag{3.12}$$

$$\dot{k}(t) = e^2(t), \;\; k(t_0) = k_0 \tag{3.13}$$

$$\widehat{y}(t) = E_o(x_1) - \widehat{x}_2(t) - \widehat{x}_3(t) - u(t)R_s \tag{3.14}$$

$$e(t) = y(t) - \widehat{y}(t) \tag{3.15}$$

Note that the use of the Mittag-Leffler function in Nussbaum functions is inpired by the previous experimental results in [49], which showed fast convergence. Simulink implementation of the Mittag-Leffler function as a Nussbaum function (i.e., equations (3.10) and (3.11) is done by using the Simulink block developed in [48]. Note that equations (3.2) - (3.15) are a form of high-gain adaptive observer [50], [51], where $N(k(t))$ is an adaptive gain which can assume high values. The following subsections provide the mathematical equations which are used for obtaining model parameters a_i. From equation (3.12) it can be seen that $u(t)$ is not affected directly by changes in the model parameters a_i. Therefore, to aid accurate modeling, the following three schemes are

presented by which the model parameters a_i can be obtained. Each scheme is observed to have certain advantages and drawbacks, which are discussed in Section 3.2.5.

3.2. Adaptive Battery Parameter Estimation Methodology: Simulated Trials

3.2.1. Scheme-1. In this scheme it is proposed that the model parameters a_i are given as follows

$$\dot{\widehat{a}}_i(t) = e^2(t) \tag{3.16}$$

where $\widehat{a}_i(0) = \widehat{a}_{i_o}$, $\widehat{a}_{i_o} > 0$ and $i = \{1,2,3...15\}$. The relationship given in equation (3.16) is chosen because $\widehat{a}_i > 0$ for all $i = \{1,2,3...15\}$.

3.2.2. Scheme-2. On considering equation (3.16), the following problem may arise. Some of the parameters $\widehat{a}_i$, $i = \{1,2,3....15\}$ may require extremely small values to obtain a reasonably accurate battery model. However, if the initial guess is even slightly off from the required small parameters values, it is possible that the resultant parameters obtained may provide an inaccurate model. In order to minimize this effect, it is proposed that the model parameters $\widehat{a}_i$ are given as follows. Let $q = \{i \in \{1,2,3...15\} : |a_i(t)| \leq \varepsilon, \varepsilon > 0, t \to \infty\}$, here, ε is a very small positive real number and t represents time. Similarly, let $\bar{q} = \{i \in \{1,2,3...15\} : |a_i(t)| > \varepsilon, \varepsilon > 0, t \to \infty\}$.

$$\dot{\widehat{a}}_i(t) = \left.\begin{array}{ll} e^2(t) + \lambda_i(\widehat{a}_{i_o} - \widehat{a}_i(t)), \lambda_i > 0 & ,i \in q \\ e^2(t) & ,i \in \bar{q} \end{array}\right\} \tag{3.17}$$

where $\widehat{a}_i(0) = a_{i_o}$, $\widehat{a}_{i_o} > 0$. The set $q = \{i \in \{1,2,3...15\} : |a_i(t)| \leq \varepsilon, \varepsilon > 0, t \to \infty\}$ identifies the indices i corresponding to which the model parameters $\widehat{a}_i$ have very small values. In equation (3.17) the term $\lambda_i \widehat{a}_{i_o}$ is used as a penalizing term to prevent model parameters $\widehat{a}_i$ from diverging from the required small magnitude by increasing the cost λ_i to a large positive number. Usually ε is easy to select because there are few battery model parameters which require extremely small values, and the order of magnitude for these values is known. The value for ε can be chosen to be similar to the

order of magnitude required for these parameters. For the parameters $\widehat{a}_i$ which do not have extremely small values, the set $\bar{q} = \{i \in \{1,2,3...15\} : |a_i(t)| > \varepsilon, \varepsilon > 0, t \to \infty\}$ identifies the indices i corresponding to which model parameters do not need the above mentioned penalization.

3.2.3. Scheme-3. To relax the requirement of having initial guesses of the model parameters close to the expected values, the following method is proposed. Let a_{iu}, a_{il} represent the upper and lower bound, respectively, for the model parameters, where $i = \{1,2,3...15\}$. Further, let λ_{x_i} be weights related to upper bounds for parameters a_i, and λ_{y_i} be weights related to lower bounds for parameters a_i. Also $a_{iu} \geq a_i \geq a_{il} > 0$ for all $i = \{1,2,3...15\}$ and $a_{iu}, a_{il} \in \mathbb{R}$. Further, $\lambda_{x_i}, \lambda_{y_i}$ are both non-negative real numbers. Then the following equation is proposed for updating the model parameters a_i:

$$\dot{\widehat{a}}_i(t) = e^2(t) + \lambda_{x_i}(a_{iu} - \widehat{a}_i(t)) + \lambda_{y_i}(a_{il} - \widehat{a}_i(t)). \tag{3.18}$$

where $\widehat{a}_i(0) = \widehat{a}_{i_o}$ and $i = \{1,2,3....15\}$. The weights λ_{x_i} and λ_{y_i} can be thought of as the user's confidence in his/her estimates of the upper and lower bounds a_{iu} and a_{il} respectively.

3.2.4. Obtaining battery model parameters. The above sections provide details related to setting up the high gain observer for battery model parameters estimation. However, due to the large number of parameters that require estimation, it is not certain that the observer shown in Figure 11 will cause the error $e(t)$ in equation (3.15) to converge to zero as time goes to infinity. To guarantee convergence of the error to zero, certain modifications need to be made to the observer structure, and the estimated parameters need to meet certain technical constraints. These details are presented in Chapter. 4.

For now, assuming the error $e(t)$ converges to zero as time goes to infinity, the following simple strategy is proposed for obtaining model parameter values $\widehat{a}_i$ from the time series of values $\widehat{a}_i(t)$, which is obtained from the adaptive parameter estimation methodology. It is observed that the model parameters $\widehat{a}_i$ converge to a constant

value and stay at that value just until before the battery dies. This can be explained from the fact that a Li-ion battery becomes unstable before its terminal voltage collapses [37]. Thus, the following equation is proposed for calculating battery model parameters $\widehat{a}_i, i = \{1,2,3....15\}$:

$$\widehat{a}_i = \frac{1}{N} \sum_{t=t_{int}}^{t_{unst}} \widehat{a}_i(t) \tag{3.19}$$

where N represents the number of samples available between time instants t_{int} and t_{unst}. Also, $t_{unst} > t_{int} > 0$; and t_{int} represents the time after which the error $e(t)$ settles within an acceptable small bound and t_{unst} represents the time after which the battery is unstable, (i.e., time after which the battery voltage begins to drop suddenly). Both time instants t_{int} and t_{unst} can be obtained by observation. Usually as per the observations, after time $t > t_{unst}$ the model parameters $\widehat{a}_i$ tend to experience small fluctuations in their values. The motivation for selecting a universal adaptive stabilizer to make the model output voltage track the terminal voltage of a real battery is as follows. From [37], it is known that as long as the battery terminal voltage stays in the region of linear decline, the battery is stable, and once the battery SOC falls below a certain value, the battery is unstable and the terminal voltage begins dropping extremely fast. To model a battery accurately, any proposed model must be able to deal with both the stable and unstable region of operation. However, making an unstable system with unknown time varying parameters track a desired reference signal is challenging. Under certain technical assumptions and constraints, universal adaptive stabilization [45] achieves such tracking. For battery modeling, it is desired that the model should be able to track sudden drops in the terminal voltage as the battery dies. Based on the above facts, a universal adaptive stabilization-based strategy is selected.

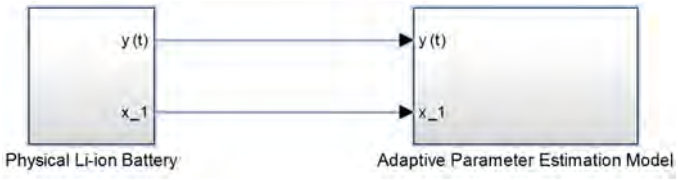

Figure 12: Simulink model for simulation

Table 1: Values of parameters $\widehat{a}_{16}$ to $\widehat{a}_{21}$ for simulation results

Parameter	$\widehat{a}_{16}$	$\widehat{a}_{17}$	$\widehat{a}_{18}$	$\widehat{a}_{19}$	$\widehat{a}_{20}$	$\widehat{a}_{21}$
Value	1.031	35	3.685	0.2156	0.1178	0.3201

3.2.5. Simulation for each scheme. In this section, simulation results related to the three adaptive parameters estimation schemes proposed in Section 3 are presented and analyzed. The simulations are performed using MATLAB and Simulink. For simulation purposes, two blocks are created in a Simulink model as shown in Figure 12.

The first block represents a physical Li-ion battery and is modeled as per equations (2.1) - (2.4). The parameters for this model are obtained from [11]. The second block assumes that the structure of the battery model is similar to Chen and Mora's model, but the parameters are unknown (i.e., uses equations (3.2) - (3.15)). The model parameters for the second block are obtained by using one of the equations (3.16), (3.17) or (3.18). Also, for all simulations a 275 mAh, 4V Li-ion battery is used. All constant load discharges for the ideal Chen and Mora model and the adaptively estimated model (using all schemes) are kept constant at 0.275A. Note that the values of parameters $\widehat{a}_{16}$ to $\widehat{a}_{21}$ are shown in Table 1, and these values are directly obtained from the parameters obtained in [11] for the $\widehat{E}_o$ given in equation (3.9).

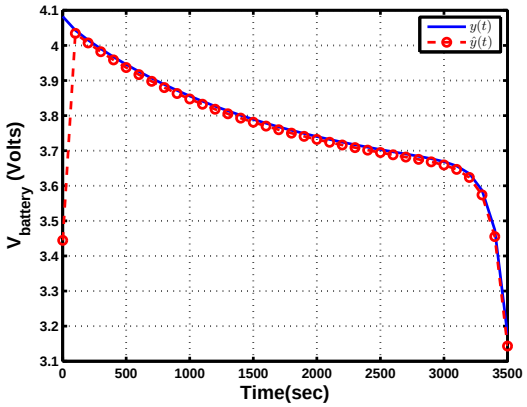

Figure 13: Comparison between $y(t)$ and $\widehat{y}(t)$ via simulation - (runtime results) (scheme-1)

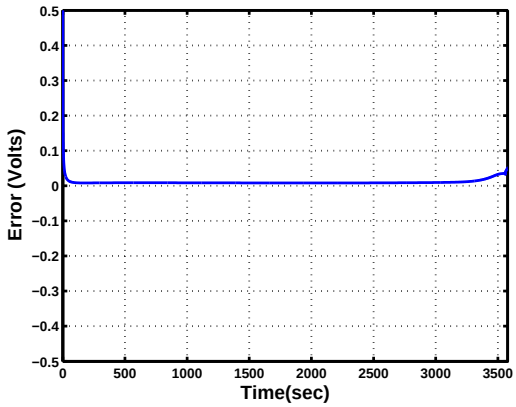

Figure 14: Error between $\widehat{y}(t)$ and $y(t)$ via simulation - (runtime results)(scheme-1)

3.2.5.1. Simulation results - scheme-1. The simulation results for an adaptive battery model parameter estimator using Scheme-1 are discussed in this section. Figure 13 shows run-time plots of the terminal voltage $y(t)$ of a physical (simulated) Li-ion battery and the terminal voltage $\widehat{y}(t)$ of the adaptively modeled battery. It can be seen from Figure 13 that the output $\widehat{y}(t)$ of the adaptively modeled battery is mostly identical to the original output $y(t)$. This verifies that the universal adaptive stabilizer based terminal voltage tracking strategy can be used for obtaining convergence of the error $e(t)$ to zero as $t \to \infty$. This is further verified by observing the plot of the error $e(t)$ in Figure 14. However, it is important to note that Figure 13 is produced by time varying parameters $\widehat{a}_i(t)$, $i \in \{1,2,3....15\}$ given as per equation (3.16). The average values for parameters $\widehat{a}_1$ to $\widehat{a}_{15}$ are determined as per the technique mentioned in Section 3.2.4 and are shown in Table 2. The above set of parameter values shown in Table 2 are used to simulate another run of a Li-ion battery model, which supplies the same constant load as used to produce Figure 13, and the output is plotted against $y(t)$ from Figure 13. This plot is shown in Figure 15. Note that these results are not runtime results, i.e. fixed estimated parameter values a_i (obtained as per Section 3.2.4) are used as opposed to the time-varying values $\widehat{a}_i(t)$ used to obtain Figure 13. It can be observed in Figure 15 that the two curves do not match. This implies that Scheme-1 can only provide a terminal voltage with the same general shape, but not with accurate numerical values. This is due to the fact that certain parameters among $\widehat{a}_1$ to $\widehat{a}_{15}$ may need to be very small but Scheme-1 has no provision to ensure this. Note that in Table 2 all parameters converge to the original values except $a_1, a_3, a_6, a_{13}, a_{15}$. This issue is fixed in the next subsection by increasing the weight of these parameters in the overall error equation. This will be further explained in the next subsection.

3.2.5.2. Simulation results - scheme-2. The simulations result for an adaptive battery model parameter estimator using Scheme-2 are discussed in this section. Note that the run-time tracking results shown in Figure 13 are a very good representation of the run-time convergence of $\widehat{y}(t)$ to $y(t)$ for all the schemes of adaptive parameter estimation presented in this work when the universal adaptive stabilizer is continuously tuning the model parameters. However, the real value of a simple usable model lies in

Table 2: Comparison of initial and final parameters ($\widehat{a}_1$ - $\widehat{a}_{15}$) (scheme-1)

Parameter	$\widehat{a}_1$	$\widehat{a}_2$	$\widehat{a}_3$	$\widehat{a}_4$	$\widehat{a}_5$
Initial Values	0.30	29	0.04	6	155
Chen and Mora's Values	0.30	29	0.04	6	155
Estimated Values	0.7607	29.4607	0.5007	6.4607	155.4607
Estimation Error (%)	153	1.5	1151	7.67	0.297
Parameter	$\widehat{a}_6$	$\widehat{a}_7$	$\widehat{a}_8$	$\widehat{a}_9$	$\widehat{a}_{10}$
Initial Values	0.04	752	13	703	6050
Chen and Mora's Values	0.04	752	13	703	6050
Estimated Values	0.5007	752.4607	13.4607	703.4607	6050.4607
Estimation Error (%)	1151.75	0.0612	3.54	0.0655	0.00761
Parameter	$\widehat{a}_{11}$	$\widehat{a}_{12}$	$\widehat{a}_{13}$	$\widehat{a}_{14}$	$\widehat{a}_{15}$
Initial Values	27	4475	0.1	24	0.07
Chen and Mora's Values	27	4475	0.1	24	0.07
Estimated Values	27.4607	4475.4	0.5607	24.4607	0.5307
Estimation Error (%)	1.7	0.0089	460.7	1.919	658.14

it's ability to have constant parameter values which can be used regardless of the battery load current. Hence, for all future schemes the run-time results are not shown. Figure 16 shows the plots of $y(t)$ obtained from an ideal Li-ion battery based upon Chen and Mora's model and $\widehat{y}(t)$ obtained based upon a model which uses the parameters shown in Table 3. The parameters shown in Table 3 represent the average values of parameters $\widehat{a}_1$ to $\widehat{a}_{15}$ obtained as given in Section 3.2.4, when parameters $\widehat{a}_1(t)$ to $\widehat{a}_{15}(t)$ are updated using equation (3.17) at run-time. For generating Figure 16, the following simulation

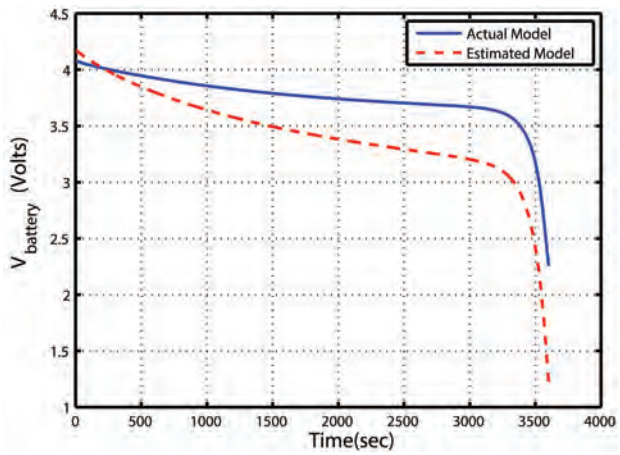

Figure 15: Battery output voltage with original parameters ($y(t)$) vs battery output voltage with estimated parameters ($\widehat{y}(t)$) - via simulation (scheme-1).

Table 3: Comparison of initial and final parameters ($\widehat{a}_1$ - $\widehat{a}_{15}$) (scheme-2)

Parameter	$\widehat{a}_1$	$\widehat{a}_2$	$\widehat{a}_3$	$\widehat{a}_4$	$\widehat{a}_5$
Initial Values	0.30	29	0.04	6	155
Chen and Mora's Values	0.30	29	0.04	6	155
Estimated Values	0.3	29.6182	0.04	6.6182	155.6182
Estimation Error (%)	0	2.13	0	10.3	0.34

Parameter	$\widehat{a}_6$	$\widehat{a}_7$	$\widehat{a}_8$	$\widehat{a}_9$	$\widehat{a}_{10}$
Initial Values	0.04	752	13	703	6050
Chen and Mora's Values	0.04	752	13	703	6050
Estimated Values	0.04	752.6182	13.6182	703.6182	6050.6
Estimation Error (%)	0	0.0822	4.755	0.0879	0.00991

Parameter	$\widehat{a}_{11}$	$\widehat{a}_{12}$	$\widehat{a}_{13}$	$\widehat{a}_{14}$	$\widehat{a}_{15}$
Initial Values	27	4475	0.1	24	0.07
Chen and Mora's Values	27	4475	0.1	24	0.07
Estimated Values	27.6182	4475.6	0.1	24.6182	0.07
Estimation Error (%)	2.289	0.0134	0	2.575	0

parameters are used: A constant discharge current of 0.275A, $\lambda_i = 100$ and $\varepsilon = 0.35$, for $i = \{1,3,6,13,15\}$; and $\lambda_i = 0$ for $i = \{2,4,5,7,8,9,10,11,12,14\}$. Note that $\lambda_i = 0$ for $i = \{2,4,5,7,8,9,10,11,12,14\}$ because these parameters have a sufficiently large value of the order of a few tens or hundreds at least hence these i's $\in \bar{q}$. The above set of parameters values shown in Table 3 are then used to simulate another run of a Li-ion battery model, supplying a constant load of 0.275A. Further, an ideal version of Chen

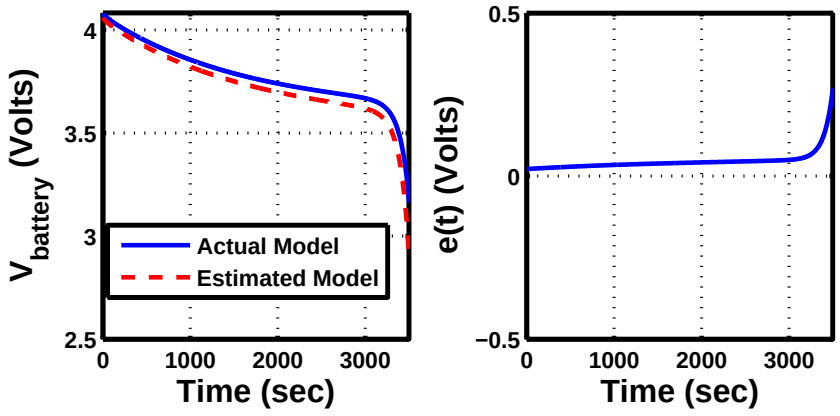

Figure 16: (Left) Battery output voltage with original parameters ($y(t)$) vs battery output voltage with estimated parameters ($\widehat{y}(t)$) - via simulation (scheme-2). (Right) Error between $\widehat{y}(t)$ and $y(t)$ via simulation - (runtime results)(scheme-2)

and Mora's model is also simulated, supplying the same constant load of 0.275A. The above simulations give $\widehat{y}(t)$ and $y(t)$ respectively, and are plotted in Figure 15. From this it is observed that Scheme-2 is successfully able to adaptively model a Li-ion battery in the presence of a constant load.

3.2.5.3. Simulation results - scheme-3. The simulations results for an adaptive battery model parameter estimator using Scheme-3 are discussed in this section. It is observed that in general parameters $\widehat{a}_1, \widehat{a}_3, \widehat{a}_6, \widehat{a}_{13}, \widehat{a}_{15}, \widehat{a}_{19}, \widehat{a}_{20}, \widehat{a}_{21}$ have very small values of the order of magnitude of 0.1. The parameters $\widehat{a}_{19}$ to $\widehat{a}_{21}$ are available from Chen and Mora's model [11]. It is further observed that if the parameters $\widehat{a}_1, \widehat{a}_3, \widehat{a}_6, \widehat{a}_{13}, \widehat{a}_{15}$ are allowed to drift far away from the order of magnitude of 0.1, then the results shown in Figure 13 are obtained. This motivated the development of Scheme-3 in Section 3.2.3, and now simulation results for this scheme are presented. As mentioned in Section 3.2.3, the proposed Scheme-3 requires upper and lower bounds to be specified for all parameters $\widehat{a}_i$ where $i = \{1,2,3...15\}$. For generating Figure 17, the following simulation parameters are used: a constant discharge current of 0.275A, $\lambda_{x_i} = 100, \lambda_{y_i} = 1$ for $i = \{1,3,6,13,15\}$; and $\lambda_{x_i} = \lambda_{y_i} = 0$ for $i = \{2,4,5,7,8,9,10,11,12,14\}$. Also for $i = \{1,3,6,13,15\}$ the upper (a_{iu}) and lower (a_{il}) bounds on the parameter values $\widehat{a}_i$ are specified in Table 4. For $i = \{2,4,5,7,8,9,10,11,12,14\}$ the upper and lower bounds are not provided because $\lambda_{x_i} = \lambda_{y_i} = 0$. $\lambda_{x_i} = \lambda_{y_i} = 0$ for $i = \{2,4,5,7,8,9,10,11,12,14\}$

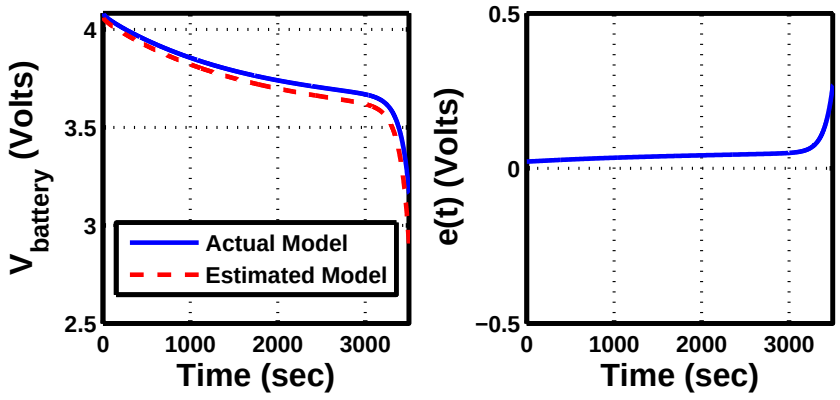

Figure 17: (Left) Battery output voltage with original parameters ($y(t)$) vs battery output voltage with estimated parameters using upper and lower bounds ($\widehat{y}(t)$) - via simulation (scheme-3). (Right) Error between $\widehat{y}(t)$ and $y(t)$ via simulation - (runtime results)(scheme-3)

is used because these parameter values are large (of the order of tens or hundreds), and Scheme-3 is not required for them. Note that Scheme-3 has been observed to work

Table 4: Upper and lower bounds and final value for parameters (scheme-3)

Parameter	$Upper\ Bound(a_{iu})$	$Lower\ Bound(a_{il})$	*Estimated Value*	*Desired Value*	$Estimation\ Error(\%)$
$\widehat{a}_1$	0.30	0.25	0.2946	0.3208	8.16
$\widehat{a}_3$	0.045	0.03	0.0443	0.04669	5.11
$\widehat{a}_6$	0.05	0.04	0.0491	0.04984	1.5
$\widehat{a}_{13}$	0.15	0.1	0.1475	0.1562	5.569
$\widehat{a}_{15}$	0.07	0.04	0.0489	0.04669	4.7

even if applied for all parameters $\widehat{a}_1$ to $\widehat{a}_{15}$. The average values for parameters $\widehat{a}_1$ to $\widehat{a}_{15}$ are determined as per the technique mentioned in Section 3.2.4 and at run-time the parameters $\widehat{a}_1(t)$ to $\widehat{a}_{15}(t)$ are updated using equation (3.18). Similar to Scheme-1 and 2, $y(t)$ and $\widehat{y}(t)$ are obtained using Scheme-3 and are shown in Figure 17.

Chapter 4: Proposed Battery Estimation Methodology and Mathematical Justification

The observations and analysis of the schemes discussed in Section 3.2 reveal several drawbacks. The drawbacks are:

1. Need of averaging at the end of parameter estimation to select estimated values of model parameters.
2. Need to start very close to the actual values of model parameters.
3. Need to have extremely tight bounds on parameter estimates.
4. Doubtful if error e(t) will converge to zero with time.

All of the above drawbacks can be overcome by altering the differential equations of the observer slightly. Thus, improved method to estimate the parameters of a Li-ion battery is proposed. This method is inspired by the Scheme-3 mentioned in Section 3.2.3. As shown in Figure 18, the following steps are proposed for estimating model parameters for a given Li-ion battery:

1. Perform a voltage relaxation test as mentioned in 5.2.1 to determine $\widehat{a}_{16}, \cdots, \widehat{a}_{21}$ by curve fitting using equation (2.10) and terminal voltage measurements so that a curve $\widehat{E}_o(\widehat{x}_1)$ is obtained such that $\widehat{E}_o(\widehat{x}_1) \approx E_o(x_1)$.
2. Perform adaptive parameter estimation with very small magnitude of discharge current i, and obtain $\widehat{a}_1, \cdots, \widehat{a}_{12}$ thus providing $\widehat{R}_{ts}$,$\widehat{R}_{tl}$,$\widehat{C}_{ts}$,$\widehat{C}_{tl}$. This process, which uses equations (3.12)-(3.15), and (3.18), is shown as **2** in Figure 18. The output equation is changed as follows for the new proposed estimation technique.

$$\widehat{y}(t) = E_o(x_1) - \widehat{x}_2(t) - \widehat{x}_3(t) \tag{4.1}$$

3. Let $i(t) \neq 0$ for all time t, compute $\widehat{R}_s$ using the estimated parameters $\widehat{a}_1$ to $\widehat{a}_{12}$ and using equation (4.2), then use curve fitting to find $\widehat{a}_{13}, \cdots, \widehat{a}_{15}$.

$$\widehat{R}_s(\widehat{x}_1(t)) = i(t)^{-1}\left(y(t) + x_2(t) + x_3(t) - E_o(\widehat{x}_1(t))\right) \tag{4.2}$$

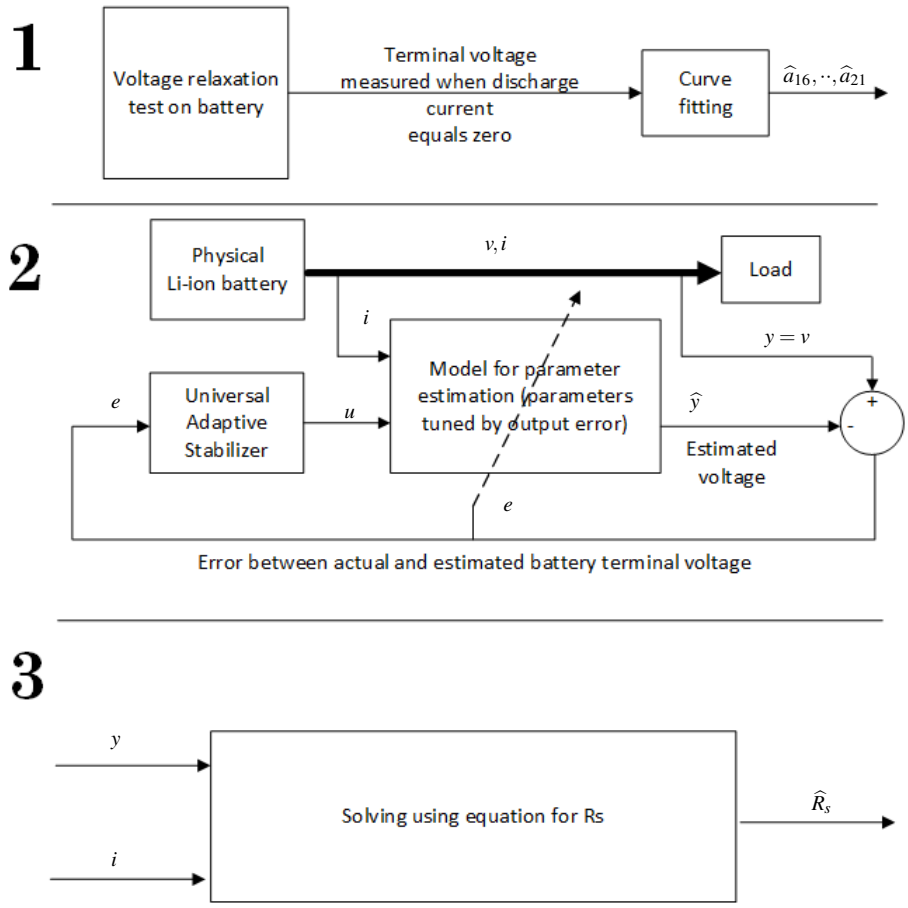

Figure 18: Steps (1,2,3) proposed for Li-ion battery model parameters estimation.

4.1. Mathematical Justification

This section shows that the process above can be used for obtaining battery model parameters. Before proving convergence of estimated model parameters to their actual values, some other results are first proved. These results are required for showing that the error $e(t)$ in equation (3.15) converges to zero.

The following result establishes conditions required to be obeyed by parameters λx_i, λy_i, a_{iu}, a_{il} where $i = \{7,9,10,12\}$.

Lemma 4.1.1. *Let* $i = \{7,9,10,12\}$. *Suppose* λ_{xi}, λ_{yi}, a_{iu}, a_{il} *are positive real numbers. Further let* $\mathbf{1} = [1 \;\; 1]^T$, $\lambda_i = [\lambda_{x_i} \;\; \lambda_{y_i}]^T$, $\mathbf{P}_i = [a_{iu} \;\; a_{il}]^T$, $1 > \varepsilon > 0$, $t > r > 0$, *then the following statements hold for* $\widehat{x}_1(t) \in [1, \varepsilon)$

1. *If* $\widehat{a}_9(0) < \widehat{a}_7(0)$, $\mathbf{1}^T\lambda_9 > \mathbf{1}^T\lambda_7$, $\mathbf{P}_9^T\lambda_9 < \mathbf{P}_7^T\lambda_7$, *and* $\widehat{a}_8(t) > -\frac{1}{\widehat{x}_1(t)} \ln\left(\frac{\widehat{a}_9(t)}{\widehat{a}_7(t)}\right)$, *then* $\widehat{C}_{ts}(\widehat{x}_1(t)) > 0$

2. *If* $\widehat{a}_{12}(0) < \widehat{a}_{10}(0)$, $\mathbf{1}^T\lambda_{12} > \mathbf{1}^T\lambda_{10}$, $\mathbf{P}_{12}^T\lambda_{12} < \mathbf{P}_{10}^T\lambda_{10}$, *and* $\widehat{a}_{11}(t) > -\frac{1}{\widehat{x}_1(t)}\ln\left(\frac{\widehat{a}_{12}(t)}{\widehat{a}_{10}(t)}\right)$, *then* $\widehat{C}_{tl}(\widehat{x}_1(t)) > 0$

Proof. Suppose that the assumptions made in the statement of Lemma 4.1.1 hold, then proceed to prove the first statement. So let $\widehat{a}_9(0) < \widehat{a}_7(0)$, $\mathbf{1}^T\lambda_9 > \mathbf{1}^T\lambda_7$, $\mathbf{P}_9^T\lambda_9 < \mathbf{P}_7^T\lambda_7$, and $\widehat{a}_8(t) > -\frac{1}{\widehat{x}_1(t)}\ln\left(\frac{\widehat{a}_9(t)}{\widehat{a}_7(t)}\right)$. The condition $\mathbf{1}^T\lambda_9 > \mathbf{1}^T\lambda_7$ implies

$$\lambda_{x_9} + \lambda_{y_9} > \lambda_{x_7} + \lambda_{y_7} \tag{4.3}$$

and $\mathbf{P}_9^T\lambda_9 < \mathbf{P}_7^T\lambda_7$ implies

$$\lambda_{x_9}a_{9u} + \lambda_{y_9}a_{9l} < \lambda_{x_7}a_{7u} + \lambda_{y_7}a_{7l} \tag{4.4}$$

Now consider $\mathscr{L}^{-1}(\widehat{A}_i(s))$, where $\widehat{A}_i(s)$ is as in equation (4.69).

$$\therefore \widehat{a}_i(t) = \widehat{a}_i(0)e^{-(\lambda_{x_i}+\lambda_{y_i})t} + (\lambda_{x_i}a_{iu} + \lambda_{y_i}a_{il})\int_{t_o}^{t} e^{-(\lambda_{x_i}+\lambda_{y_i})\tau}d\tau + \int_{t_o}^{t} e^2(t-\tau)e^{-(\lambda_{x_i}+\lambda_{y_i})\tau}d\tau \tag{4.5}$$

Now since $\lambda_{x_9} + \lambda_{y_9} > \lambda_{x_7} + \lambda_{y_7}$ and $0 < \widehat{a}_9(0) < \widehat{a}_7(0)$ then by properties of the function e^x, the following can be written

$$\widehat{a}_9(0)e^{-(\lambda_{x_9}+\lambda_{y_9})t} < \widehat{a}_9(0)e^{-(\lambda_{x_7}+\lambda_{y_7})t} < \widehat{a}_7(0)e^{-(\lambda_{x_7}+\lambda_{y_7})t}, t > t_0 \tag{4.6}$$

From the above it also follows that

$$\int_{t_o}^{t} e^{-(\lambda_{x_9}+\lambda_{y_9})\tau}d\tau < \int_{t_o}^{t} e^{-(\lambda_{x_7}+\lambda_{y_7})\tau}d\tau, t > t_0 \tag{4.7}$$

and further using equation (4.4), (4.7) together provides

$$\begin{aligned}(\lambda_{x_9}a_{9u} + \lambda_{y_9}a_{9l})\int_{t_o}^{t} e^{-(\lambda_{x_9}+\lambda_{y_9})\tau}d\tau < (\lambda_{x_9}a_{9u} + \lambda_{y_9}a_{9l})\int_{t_o}^{t} e^{-(\lambda_{x_7}+\lambda_{y_7})\tau}d\tau \cdots \\ \cdots < (\lambda_{x_7}a_{7u} + \lambda_{y_7}a_{7l})\int_{t_o}^{t} e^{-(\lambda_{x_7}+\lambda_{y_7})\tau}d\tau\end{aligned} \tag{4.8}$$

Similarly utilizing properties of the exponential function, using equation (4.3) and recognizing that $e^2(t-\tau) > 0$ for all t, the following can be written.

$$\int_{t_o}^{t} e^2(t-\tau)e^{-(\lambda_{x_9}+\lambda_{y_9})\tau}d\tau < \int_{t_o}^{t} e^2(t-\tau)e^{-(\lambda_{x_7}+\lambda_{y_7})\tau}d\tau \tag{4.9}$$

$\therefore$ Using equations (4.5), (4.6), (4.8) and (4.9) provides

$$\widehat{a}_9(t) < \widehat{a}_7(t), \text{ for all } t > t_0 \tag{4.10}$$

$\therefore$ From above $\frac{\widehat{a}_9(t)}{\widehat{a}_7(t)} < 1$, $\therefore \ln\left(\frac{\widehat{a}_9(t)}{\widehat{a}_7(t)}\right) < 0. \therefore \ -\ln\left(\frac{\widehat{a}_9(t)}{\widehat{a}_7(t)}\right) > 0$, and also for $\widehat{x}_1(t) \in [1,0)$

$$-\frac{1}{\widehat{x}_1(t)}\ln\left(\frac{\widehat{a}_9(t)}{\widehat{a}_7(t)}\right) > 0 \tag{4.11}$$

However,

$$-\frac{1}{\widehat{x}_1(t)}\ln\left(\frac{\widehat{a}_9(t)}{\widehat{a}_7(t)}\right) < \widehat{a}_8(t) \tag{4.12}$$

$$-\ln\left(\frac{\widehat{a}_9(t)}{\widehat{a}_7(t)}\right) < \widehat{x}_1(t)\widehat{a}_8(t) \tag{4.13}$$

$$\widehat{x}_1(t) > \frac{-1}{\widehat{a}_8(t)}\ln\left(\frac{\widehat{a}_9(t)}{\widehat{a}_7(t)}\right) > 0 \tag{4.14}$$

$$-\widehat{x}_1(t)\widehat{a}_8(t) < \ln\left(\frac{\widehat{a}_9(t)}{\widehat{a}_7(t)}\right) \tag{4.15}$$

$$e^{-\widehat{x}_1(t)\widehat{a}_8(t)} < \frac{\widehat{a}_9(t)}{\widehat{a}_7(t)} \tag{4.16}$$

$$\Rightarrow -\widehat{a}_7(t)e^{-\widehat{x}_1(t)\widehat{a}_8(t)} > -\widehat{a}_9(t) \tag{4.17}$$

$$\therefore -\widehat{a}_7(t)e^{-\widehat{x}_1(t)\widehat{a}_8(t)} + \widehat{a}_9(t) > 0 \tag{4.18}$$

By definition of $\widehat{C}_{ts}$ and from equation (4.18), $\widehat{C}_{ts} > 0$

This completes the proof of the first statement. For statement two, the above steps are to be repeated by replacing $\widehat{a}_9(0)$ by $\widehat{a}_{12}(0)$, $\widehat{a}_7(0)$ by $\widehat{a}_{10}(0)$, λ_9 by λ_{12}, λ_7 by λ_{10}, $\mathbf{P}_9$ by $\mathbf{P}_{12}$, $\mathbf{P}_7$ by $\mathbf{P}_{10}$ and $\widehat{a}_8$ by $\widehat{a}_{11}$ and following the exact same steps as above;

hence the process has not been repeated. However, following the above mentioned steps leads to the complete proof. The theorem presented below proves the convergence of the estimated parameters to the actual parameters if all the conditions explained in Lemma 4.1.1 are satisfied. □

Theorem 4.1.2. *Suppose that the conditions required for Lemma 4.1.1 to hold are satisfied. Further assume that the voltage relaxation test described in Section 5.2.1 provides* $\widehat{E}_0(\widehat{x}_1) = E_0(x_1)$. *Let* $e(t) = y(t) - \widehat{y}(t)$, *where* $y(t)$, $\widehat{y}(t)$ *are given by equation* (2.4) *and* (3.14) *respectively. If the discharge current* $i(t)$ *is an infinitesimally small positive number, then as* $t \to \infty$

1. $\widehat{R}_{ts}(\widehat{x}_1)\widehat{C}_{ts}(\widehat{x}_1) = R_{ts}C_{ts}$.
2. $\widehat{R}_{tl}(\widehat{x}_1)\widehat{C}_{tl}(\widehat{x}_1) = R_{tl}C_{tl}$.

Proof. Suppose that the assumptions mentioned in the statement of this theorem are satisfied. Note that in this proof the arguments of functions are not written for convenience.

Let

$$y_1 = -x_2 - x_3 \tag{4.19}$$

and

$$\widehat{y}_1 = -\widehat{x}_2 - \widehat{x}_3 \tag{4.20}$$

Since $\widehat{E}_0(\widehat{x}_1) = E_0(x_1)$, and $i(t) \to 0$

$$e = y - \widehat{y} = y_1 - \widehat{y}_1 \tag{4.21}$$

Taking derivatives of both sides gives

$$\dot{e} = \dot{y}_1 - \dot{\widehat{y}}_1 \tag{4.22}$$

Now add and subtract e to the R.H.S.

$$\dot{e} = -e + e + \dot{y}_1 - \dot{\widehat{y}}_1 \tag{4.23}$$

$$\dot{e} = -e + y_1 - \widehat{y}_1 + \dot{y}_1 - \dot{\widehat{y}}_1 \tag{4.24}$$

Now rearrange terms to get

$$\dot{e} = -e - \dot{\widehat{y}}_1 - \widehat{y}_1 + (y_1 + \dot{y}_1) \tag{4.25}$$

Let

$$S(t) = y_1 + \dot{y}_1 \tag{4.26}$$

Therefore from equations (3.14), (4.25) and (4.26)

$$\dot{e} = -e + \dot{\widehat{x}}_2 + \dot{\widehat{x}}_3 - \widehat{y}_1 + S \tag{4.27}$$

Now by equations (3.2), (3.3), and (3.14)

$$\therefore \dot{e} = -e - \frac{\widehat{x}_2}{\widehat{R}_{ts}\widehat{C}_{ts}} - \frac{\widehat{x}_3}{\widehat{R}_{tl}\widehat{C}_{tl}} + 2u + \widehat{x}_2 + \widehat{x}_3 + S \tag{4.28}$$

$$\dot{e} = -e + 2u + \widehat{x}_2\left(1 - \frac{1}{\widehat{R}_{ts}\widehat{C}_{ts}}\right) + \widehat{x}_3\left(1 - \frac{1}{\widehat{R}_{tl}\widehat{C}_{tl}}\right) + S \tag{4.29}$$

Since the conditions required for the Lemma 4.1.1 to hold are satisfied $\therefore$ by Lemma 4.1.1, $\widehat{C}_{ts} > 0$, $\widehat{C}_{tl} > 0$. Also $\widehat{R}_{ts} > 0$, $\widehat{R}_{tl} > 0$ by definition in equation (2.6) and (2.5). $\therefore \widehat{R}_{ts}\widehat{C}_{ts} > 0$, $\widehat{R}_{tl}\widehat{C}_{tl} > 0$, So it is possible to write

$$\frac{1}{\widehat{R}_{ts}\widehat{C}_{ts}} > 0 \tag{4.30}$$

$$1 - \frac{1}{\widehat{R}_{ts}\widehat{C}_{ts}} < 1 \tag{4.31}$$

$$\widehat{x}_2\left(1-\frac{1}{\widehat{R}_{ts}\widehat{C}_{ts}}\right)<\widehat{x}_2 \tag{4.32}$$

Similarly since $\widehat{R}_{tl}\widehat{C}_{tl}>0$ and following the procedure in equations (4.30), (4.31), and (4.32) gives

$$\widehat{x}_3\left(1-\frac{1}{\widehat{R}_{tl}\widehat{C}_{tl}}\right)<\widehat{x}_3 \tag{4.33}$$

From equations (4.32) and (4.33) it follows that

$$-\widehat{x}_2\left(1-\frac{1}{\widehat{R}_{ts}\widehat{C}_{ts}}\right)>-\widehat{x}_2 \tag{4.34}$$

$$-\widehat{x}_3\left(1-\frac{1}{\widehat{R}_{tl}\widehat{C}_{tl}}\right)>-\widehat{x}_3 \tag{4.35}$$

$\therefore$ from the above

$$-\widehat{x}_2\left(1-\frac{1}{\widehat{R}_{ts}\widehat{C}_{ts}}\right)-\widehat{x}_3\left(1-\frac{1}{\widehat{R}_{tl}\widehat{C}_{tl}}\right)>-\widehat{x}_2-\widehat{x}_3 \tag{4.36}$$

From equations (3.14) and (4.36)

$$\widehat{y}_1<-\widehat{x}_2\left(1-\frac{1}{\widehat{R}_{ts}\widehat{C}_{ts}}\right)-\widehat{x}_3\left(1-\frac{1}{\widehat{R}_{tl}\widehat{C}_{tl}}\right) \tag{4.37}$$

$$\therefore -\widehat{y}_1>\widehat{x}_2\left(1-\frac{1}{\widehat{R}_{ts}\widehat{C}_{ts}}\right)+\widehat{x}_3\left(1-\frac{1}{\widehat{R}_{tl}\widehat{C}_{tl}}\right) \tag{4.38}$$

$$y_1-\widehat{y}_1>y_1+\widehat{x}_2\left(1-\frac{1}{\widehat{R}_{ts}\widehat{C}_{ts}}\right)+\widehat{x}_3\left(1-\frac{1}{\widehat{R}_{tl}\widehat{C}_{tl}}\right) \tag{4.39}$$

$\therefore$ From equation (3.15)

$$e>y_1+\widehat{x}_2\left(1-\frac{1}{\widehat{R}_{ts}\widehat{C}_{ts}}\right)+\widehat{x}_3\left(1-\frac{1}{\widehat{R}_{tl}\widehat{C}_{tl}}\right) \tag{4.40}$$

Adding $-e+2u+\dot{y}_1$ to both sides gives

$$-e+2u+\dot{y}_1+e>-e+2u+\dot{y}_1+y_1+\widehat{x}_2\left(1-\frac{1}{\widehat{R}_{ts}\widehat{C}_{ts}}\right)+\widehat{x}_3\left(1-\frac{1}{\widehat{R}_{tl}\widehat{C}_{tl}}\right) \tag{4.41}$$

$\therefore$ From equations (4.26) and (4.29)

$$2u + \dot{y}_1 > \dot{e}(t) \tag{4.42}$$

$$\dot{e}(t) < 2u + \dot{y}_1 \tag{4.43}$$

Now consider

$$V(e,k) = \frac{1}{2}e^2(t) + 2\int_{k(t_0)}^{k(t)} N(\tau)d\tau \tag{4.44}$$

Taking the time derivative of equation (4.44) gives

$$\dot{V} = e\dot{e} + 2N(k(t))\dot{k}(t) \tag{4.45}$$

$$\dot{V} = e\dot{e} + 2N(k(t))e^2(t) \tag{4.46}$$

From equations (4.43) and (4.46)

$$\dot{V} = e(2u + \dot{y}_1 + 2N(k(t))e^2(t) \tag{4.47}$$

Now since $u = -N(k(t))e(t)$

$$\therefore \dot{V} < -2N(k(t))e^2(t) + e\dot{y}_1 + 2N(k(t))e^2(t) \tag{4.48}$$

$$\therefore \dot{V} < e\dot{y}_1 \tag{4.49}$$

Consider the following for any value of e, $\dot{y}_1$

$$(e - \dot{y}_1)^2 > 0 \tag{4.50}$$

$$e^2 - 2e\dot{y}_1 + \dot{y}_1^2 > 0 \tag{4.51}$$

$$\therefore e\dot{y}_1 < \frac{1}{2}(e^2 + \dot{y}_1^2) \tag{4.52}$$

From equations (4.49) and (4.52)

$$\dot{V} < \frac{1}{2}e^2 + \frac{1}{2}\dot{y}_1^2 \tag{4.53}$$

Integrating the above from t_0 to t gives

$$V(t) - V(t_0) < \frac{1}{2}\int_{t_o}^{t} e^2(\tau)d\tau + \frac{1}{2}\int_{t_o}^{t} \dot{y}_1^2(\tau)d\tau \tag{4.54}$$

Substituting equation (4.44) into equation (4.54) gives

$$\frac{1}{2}e^2(t) + 2\int_{k(t_0)}^{k(t)} N(\tau)d\tau - V(t_0) < \frac{1}{2}\int_{t_o}^{t} e^2(\tau)d\tau + \frac{1}{2}\int_{t_o}^{t} \dot{y}_1^2(\tau)d\tau \tag{4.55}$$

$$\therefore \frac{1}{2}e^2(t) < \frac{1}{2}\int_{t_o}^{t} e^2(\tau)d\tau + \frac{1}{2}\int_{t_o}^{t} \dot{y}_1^2(\tau)d\tau - 2\int_{k(t_0)}^{k(t)} N(\tau)d\tau + V(t_0) \tag{4.56}$$

By definition of $\dot{k}(t)$ in equation (3.13)

$$\frac{1}{2}e^2(t) < \frac{1}{2}k(t) - \frac{1}{2}k(t_0) + \frac{1}{2}\int_{t_o}^{t} \dot{y}_1^2(\tau)d\tau - 2\int_{k(t_0)}^{k(t)} N(\tau)d\tau + V(t_0) \tag{4.57}$$

Dividing both sides by $\frac{1}{2}(k(t) - k(t_0))$

$$\frac{1}{(k(t)-k(t_0))}e^2(t) < 1 + \frac{1}{(k(t)-k(t_0))}\int_{t_o}^{t} \dot{y}_1^2(\tau)d\tau - \frac{4}{(k(t)-k(t_0))}\int_{k(t_0)}^{k(t)} N(\tau)d\tau + \cdots$$
$$\cdots \frac{2}{(k(t)-k(t_0))}V(t_0) \tag{4.58}$$

Now by the definition of y, y_1 in equation (2.4) and (4.19)

$$y_1 = y - E_0 + iR_s \tag{4.59}$$

$$\dot{y}_1 = \dot{y} - \frac{\partial E}{\partial x_1} + R_s\frac{di}{dt} + i\frac{dR_s}{dt} \tag{4.60}$$

Using equation (2.10) in equation (4.60)

$$\dot{y}_1 = \dot{y} + \frac{i(t)}{C_c}(a_{16}a_{17}e^{-a_{17}x_1} + a_{19} - 2a_{20}x_1 + 3a_{21}x_1^2) + R_s\frac{di}{dt} + i\frac{dR_s}{dt} \tag{4.61}$$

Now using equation (2.9)

$$\dot{y}_1 = \dot{y} + \frac{i(t)}{C_c}(a_{16}a_{17}e^{-a_{17}x_1} + a_{19} - 2a_{20}x_1 + 3a_{21}x_1^2) + R_s\frac{di}{dt} + \frac{i(t)^2}{C_c}(a_{13}a_{14}e^{-a_{14}x_1}) \tag{4.62}$$

Now consider that $t \to \infty$. Every battery can supply current for a certain amount of time, say $T > t_0$. For all $t > T$, $i(t) = 0$, $y(t) = 0$, $x_1(t) = 0$ and $\therefore$ for $t > T$, $\dot{y}(t) = 0$, $i(t) = 0$.

Using the above facts with equation (4.62) gives the fact that there exists some time $T > t_0$ such that for all $t > T$, $\dot{y}(t) = 0$. Also note that in reality the terminal voltage may have spikes however $\dot{y}(t)$ cannot practically be infinite (even if a battery short circuit occurs).

$\therefore \dot{y}_1(t)$ in equation (4.62) is bounded and goes to zero as time progresses. Therefore $\int_{t_o}^{t} \dot{y}_1^2(\tau)d\tau$ is bounded.

Now suppose that $k(t) \to \infty$ as $t \to \infty$; and based on the above discussion and using equation (4.58)

$$\lim_{t\to\infty} \frac{1}{(k(t) - k(t_0))}e^2(t) < -\frac{4}{(k(t) - k(t_0))}\int_{k(t_0)}^{k(t)} N(\tau)d\tau \tag{4.63}$$

Now if $k(t) \to \infty$ as $t \to \infty$ then by the definition of a Nussbaum function in equation (3.10) the R.H.S of equation (4.63) can take values approaching $-\infty$, and therefore this will violate equation (4.63) as considering the definition of $k(t)$ in equation (3.13), the L.H.S of equation (4.63) is positive, and $k(t) \to \infty$ leads to a positive number less than a negative number.

By this contradiction, the assumption that $k(t) \to \infty$ is false and therefore $k(t)$ is bounded. However $\dot{k}(t)$ is a non decreasing function by definition and $k(t)$ is bounded. This implies that $k(t) \to k_\infty$ as $t \to \infty$ which further implies that $\dot{k}(t) \to 0$ as $t \to \infty$, i.e. $e^2(t) \to 0$ as $t \to \infty$ or $e(t) \to 0$ as $t \to \infty$, i.e. $y_1 \to \widehat{y}_1$ as $t \to \infty$.

Consider now that $y_1 \to \widehat{y}_1$, which implies that

$$-x_2 - x_3 = -\widehat{x}_2 - \widehat{x}_3 \tag{4.64}$$

$$[-1 \quad -1]\left(\begin{bmatrix} x_2 \\ x_3 \end{bmatrix} - \begin{bmatrix} \widehat{x}_2 \\ \widehat{x}_3 \end{bmatrix}\right) = 0 \tag{4.65}$$

The above implies $x_2 = \widehat{x}_2$, $x_3 = \widehat{x}_3$ and therefore also means that $\dot{x}_2 = \dot{\widehat{x}}_2$ and $\dot{x}_3 = \dot{\widehat{x}}_3$.

Let's consider $\dot{x}_2 = \dot{\widehat{x}}_2$, which is written using equations (3.2) and (2.2) as

$$-\frac{x_2(t)}{R_{ts}(x_1)C_{ts}(x_1)} + \frac{i(t)}{C_{ts}(x_1)} = -\frac{\widehat{x}_2(t)}{\widehat{R}_{ts}(\widehat{x}_1)\widehat{C}_{ts}(\widehat{x}_1)} + u(t) \tag{4.66}$$

Since it is proved above that $e(t) \to 0$ as $t \to \infty$, $u(t) = -N(k(t))e(t)$, $i(t)$ is infinitesimally small, and $x_2(t) = \widehat{x}_2(t)$.

$\therefore$ all the terms in equation (4.66) cancel out providing

$$\widehat{R}_{ts}\widehat{C}_{ts} = R_{ts}C_{ts} \tag{4.67}$$

Considering $\dot{x}_3 = \dot{\widehat{x}}_3$ and following exactly the same arguments as above, it is similarly possible to conclude that $\widehat{R}_{tl}\widehat{C}_{tl} = R_{tl}C_{tl}$. This completes the proofs of the two required results. □

The above result proves that as long as the discharge current has a very small value, the magnitude of the product of estimated RC pairs $\widehat{R}_{ts}\widehat{C}_{ts}$ will equal the product of the actual RC pairs $R_{ts}C_{ts}$, regardless of the values to which the constants $\widehat{a}_1, \cdots, \widehat{a}_{12}$ converge. Now we proceed to prove that the constants $\widehat{a}_1$ to $\widehat{a}_{12}$ converge.

Lemma 4.1.3. *Let $\dot{\widehat{a}}_i(t)$ be defined by equation* (3.18) *then $\widehat{a}_i(t) \to \frac{\lambda_{xi}a_{iu}+\lambda_{yi}a_{il}}{\lambda_{xi}+\lambda_{yi}}$ as $t \to \infty$, where λ_{xi}, λ_{yi}, a_{iu}, a_{il} are positive real numbers.*

Proof. Taking the Laplace transform of equation (3.18) and rearranging terms gives.

$$s\widehat{A}_i(s) - \widehat{a}_i(0) = L[e^2(t)] + \frac{\lambda_{x_i}a_{iu} + \lambda_{y_i}a_{il}}{s} - (\lambda_{x_i} + \lambda_{y_i})\widehat{A}_i(s) \tag{4.68}$$

$$\widehat{A}_i(s) = \frac{L[e^2(t)]}{(s + \lambda_{x_i} + \lambda_{y_i})} + \frac{\widehat{a}_i(0)}{(s + \lambda_{x_i} + \lambda_{y_i})} + \frac{\lambda_{xi}a_{iu} + \lambda_{y_i}a_{il}}{s(s + \lambda_{x_i} + \lambda_{y_i})} \tag{4.69}$$

Now applying final value theorem to equation (4.69) provides the following.

$$\lim_{t\to\infty} \widehat{a}_i(t) = \lim_{s\to 0} s\widehat{A}_i(s) = \frac{\lambda_{x_i}a_{iu} + \lambda_{y_i}a_{il}}{\lambda_{x_i} + \lambda_{y_i}} \tag{4.70}$$

Therefore from equation (4.70) the required results are proved. □

Algorithm 1 Adaptive Li-ion battery parameter estimation algorithm (pseudocode)

- **Physical requirements:** A fully charged Li-ion battery, appropriate discharging, data acquisition circuitry.
- **Data:** Initial time t_0, time step t_{step}, termination time t_{max}. Parameters $\widehat{a}_{16}, \cdots, \widehat{a}_{21}$ from 'Step 1' of the procedure in Section 4. Parameters $\widehat{a}_i(t_0)$, a_{iu}, a_{il}, λ_{xi}, λ_{yi} for $i \in \{1, \cdots, 12\}$ satisfying conditions required for Lemma 4.1.1 to hold. Very small positive discharge current $\mathbf{i}(t)$ for $t \geq t_0$. Adaptive tracking error bound $\varepsilon_2 > 0$. Initial conditions $\widehat{x}_1(t_0) = 1$, $\widehat{x}_2(t_0) = \widehat{x}_3(t_0) = \widehat{y}(t_0) = 0$, battery Ah capacity C.
- **Output:** Estimated battery parameters $[\widehat{a}_1, \cdots, \widehat{a}_{12}]$.

for $t = t_0 : t_{step} : t_{max}$ **do**
    Read measured battery terminal voltage y, battery discharge current $\mathbf{i}$.
    Calculate $e = y - \widehat{y}$
    Find u as per equation (3.12).
    Get estimated battery parameters $\widehat{a}_i$ according to equation (3.18) for $i \in \{1, \cdots, 12\}$.
    Compute state estimates $\widehat{x}_1, \cdots, \widehat{x}_3$ using equations (3.2)-(3.3).
    Update estimated battery terminal voltage $\widehat{y}$ using equation (4.1).
    if $e < \varepsilon_2$ **then**
        Return $[\widehat{a}_1, \cdots, \widehat{a}_{12}]$
        Continue loop execution
    else
        Return Null
        Continue loop execution
    end if
end for

Lemma 4.1.3 shows that the parameters $\widehat{a}_i(t)$ for $i = \{1, \cdots 12\}$ converge to values depending upon the choices of the weights λ_{x_i}, λ_{y_i} and the upper and lower bounds a_{iu} and a_{il}. Note that Lemma 4.1.3 only guarantees convergence of $\widehat{a}_i(t)$ for $i = \{1, \cdots 12\}$, however, it does not guarantee that $\widehat{a}_i(t)$ convergence to the correct values. Further, it is shown that this does not hinder extracting parameters $\widehat{R}_{ts}(x_1)$, $\widehat{R}_{tl}(x_1)$, $\widehat{C}_{ts}(x_1)$, $\widehat{C}_{tl}(x_1)$ accurately.

The error in estimation depends on the choice of upper and lower bounds. Suppose $\widehat{C}_{ts} = C_{ts} + \Delta$, where Δ is the error in estimation of model parameters due to the assumption that $i(t) \to 0$ or due to improper choice of upper and lower bounds.

From the theorem $\widehat{R}_{ts}\widehat{C}_{ts} = R_{ts}C_{ts}$

$$\therefore \widehat{R}_{ts} = \frac{R_{ts}C_{ts}}{\widehat{C}_{ts} + \Delta} = \frac{R_{ts}}{1 + \frac{\Delta}{C_{ts}}} \tag{4.71}$$

The equation (4.71) provides an approximation of estimation error of R_{ts} in terms of error in estimating C_{ts}. Similarly the following equation can be written.

$$\therefore \widehat{R}_{tl} = \frac{R_{tl}C_{tl}}{\widehat{C}_{tl}+\Delta} = \frac{R_{tl}}{1+\frac{\Delta}{C_{tl}}} \tag{4.72}$$

The estimation procedure is shown in pseudo code presented in Algorithm 1.

4.1.1. Simulation results. This section comprises of simulation results using the improved estimation method discussed in Section 4. In the simulation case, the parameters $\widehat{a}_{16}$ to $\widehat{a}_{21}$ are already obtained as previously shown in Table 1, which are extracted from the data given in [11]. Now that the parameters $\widehat{a}_{16}$ to $\widehat{a}_{21}$ are obtained, the next step is to use the estimation technique to get parameters $\widehat{a}_1$ to $\widehat{a}_{12}$, whereas parameters $\widehat{a}_{13}$ to $\widehat{a}_{15}$ will be obtained at the end using a separate calculation method. For the parameters $\widehat{a}_1$ to $\widehat{a}_{12}$, the conditions mentioned in Lemma 4.1.1 are strictly followed, which assures convergence as already validated in Section 4.1. Note that there are some stability conditions that need to be met, and these conditions inform about when the estimation needs to be stopped, so that the estimated values don't give an

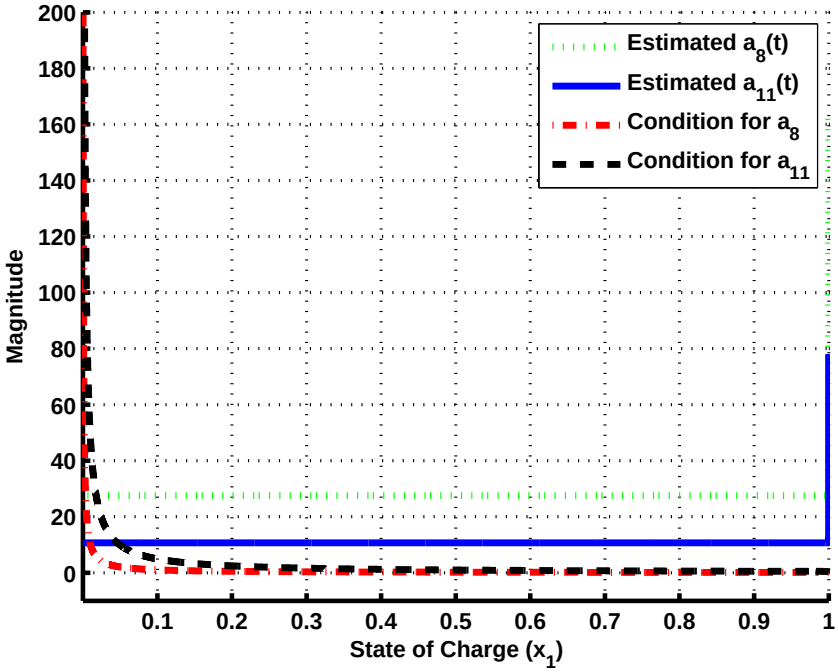

Figure 19: Intersection point of $\widehat{a}_8$ and $\widehat{a}_{11}$ with their respective stability conditions.

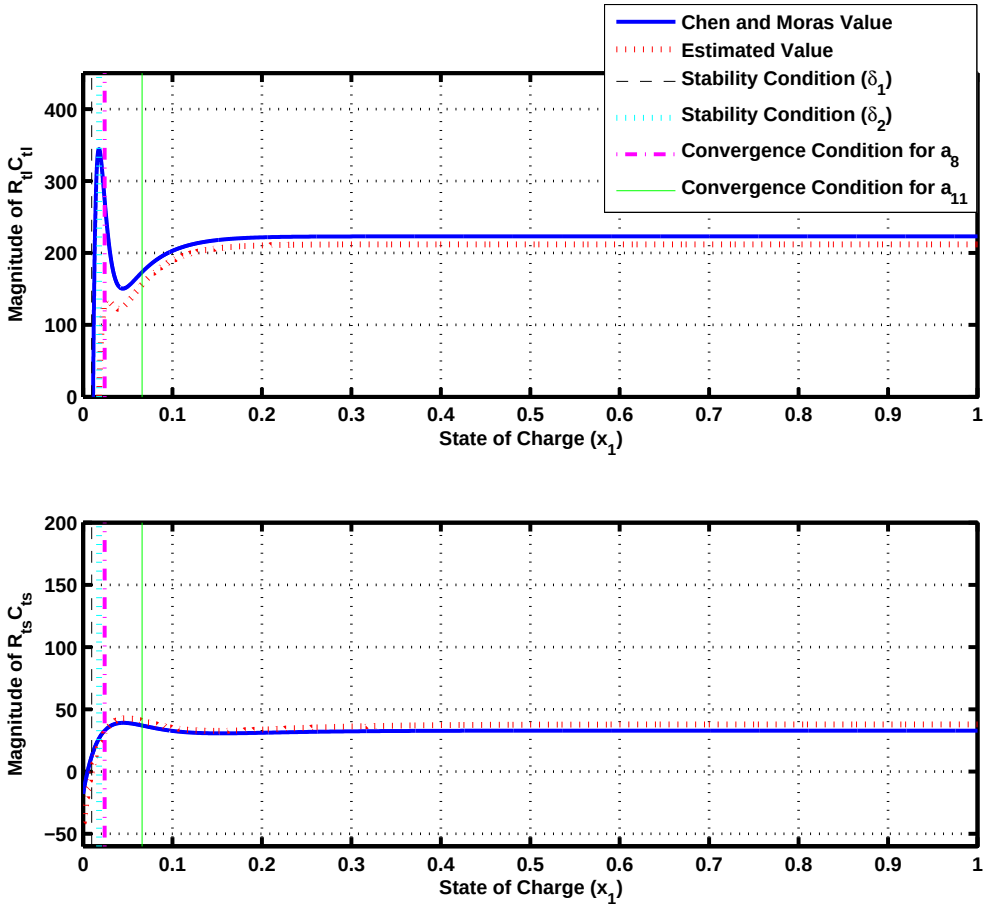

Figure 20: $\widehat{R}_{ts}\widehat{C}_{ts}$ and $\widehat{R}_{tl}\widehat{C}_{tl}$ plots of estimated parameters versus Chen and Mora's parameters (Simulation Results)

unstable model. Note that in all the plots, the dashed vertical line shows the stability condition $\delta_1 = -\frac{1}{\widehat{a}_8}\ln\left(\frac{\widehat{a}_9}{\widehat{a}_7}\right)$, the dotted vertical line shows the stability condition

Table 5: Simulation results for estimated parameters

Parameter	*Upper Bound*(a_{iu})	*Lower Bound*(a_{il})	λ_{x_i}	λ_{y_i}	*Initial Value*	*Estimated Value*	*Desired Value*	*Estimation Error*(%)
$\widehat{a}_1$	1	0.1	50	50	180	0.5555	0.3208	42.25
$\widehat{a}_2$	50	10	50	50	17	29.9996	29.14	2.86
$\widehat{a}_3$	0.1	0.01	50	50	24	0.0557	0.04669	16.17
$\widehat{a}_4$	10	1	50	50	3600	5.6095	6.603	17.71
$\widehat{a}_5$	200	100	50	50	93	149.9983	155.2	3.47
$\widehat{a}_6$	0.1	0.01	50	50	264	0.0630	0.04984	20.88
$\widehat{a}_7$	1000	500	60	55	510	759.2573	752.9	0.837
$\widehat{a}_8$	30	1	50	10	78	10.6712	13.51	26.6
$\widehat{a}_9$	800	500	80	50	451	684.61	703.6	2.77
$\widehat{a}_{10}$	7000	5000	10	10	420	5999.6	6056	0.94
$\widehat{a}_{11}$	50	5	50	50	162	27.5014	27.12	1.386
$\widehat{a}_{12}$	5000	3000	10	20	363	3666.6	4475	22.04

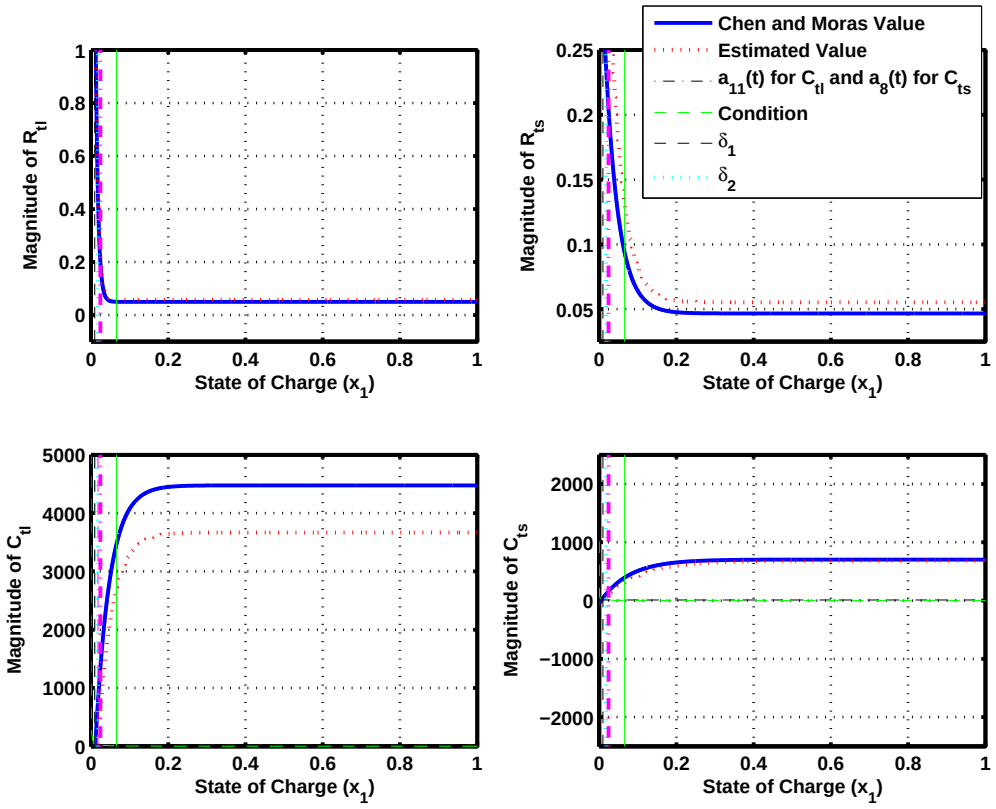

Figure 21: (Top Left) Plot for $\widehat{R}_{tl}$ with required stability conditions (simulation result). (Top Right) Plot for $\widehat{R}_{ts}$ with required stability conditions (simulation result). (Bottom Left) Plot for $\widehat{C}_{tl}$ with required stability conditions (simulation result). (Bottom Right) Plot for $\widehat{C}_{ts}$ with required stability conditions (simulation result).

$\delta_2 = -\frac{1}{\widehat{a}_{11}} \ln\left(\frac{\widehat{a}_{12}}{\widehat{a}_{10}}\right)$. The dashed-dotted vertical line shows the state of charge point found by the intersection of a_8 found by using adaptive technique and the stability condition $-\frac{1}{\widehat{x}_1(t)} \ln\left(\frac{\widehat{a}_9(t)}{\widehat{a}_7(t)}\right)$ while the solid vertical line shows the state of charge point found by the intersection of $\widehat{a}_{11}$ found by using adaptive technique and the stability condition $-\frac{1}{\widehat{x}_1(t)} \ln\left(\frac{\widehat{a}_{12}(t)}{\widehat{a}_{10}(t)}\right)$. In all the plots presented in the simulation section as well as the experimentation section, the vertical lines show the limits of these stability conditions. The estimation technique needs to be stopped before these values are reached by the parameters. If estimation is not stopped before these stability conditions are reached, the model becomes unstable and the parameters extracted give unstable model. Once the adaptive technique discussed in Section 4 is implemented, the intersection points of $\widehat{a}_8$ and $\widehat{a}_{11}$ are found respectively for their stability conditions. This is presented in Figure 19. After obtaining the points of the state of charge for each intersection, these

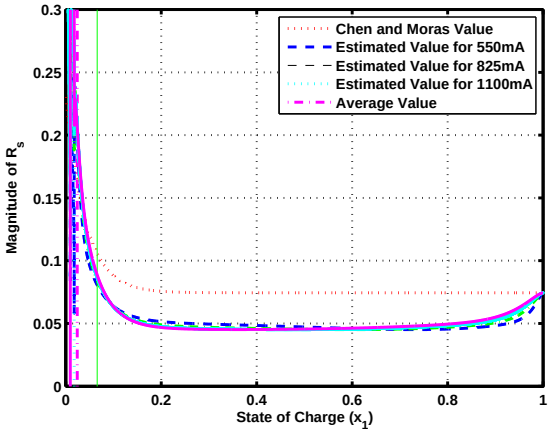

Figure 22: Calculated $\widehat{R}_s$ values for different currents in comparison with Chen and Mora's values

points can be used to plot the vertical lines, which will show the criteria to stop the estimation algorithm. Note that the proof discussed in Section 4.1 suggests that the product $\widehat{R}_{tl}\widehat{C}_{tl}$ and $\widehat{R}_{ts}\widehat{C}_{ts}$ converges even if the estimates of the individual parameters ($\widehat{R}_{tl}$, $\widehat{R}_{ts}$, $\widehat{C}_{tl}$, and $\widehat{C}_{ts}$) do not converge to the actual values independently by themselves, which can be observed in Figure 20. This implies that even if there is some error in estimating either the resistances or capacitances, the product of estimated resistance and capacitance converges to the true value of the product, thus the battery model dynamics can be replicated reasonably well by using the estimated parameters. Further, if bound on either the resistance or the capacitance values are known then the estimation of the individual parameters can be improved. The individual plots for $\widehat{R}_{tl}$, $\widehat{R}_{ts}$, $\widehat{C}_{tl}$, and $\widehat{C}_{ts}$ are shown in Figure 21. Once these parameters are obtained, the only thing left is to find the parameters for $\widehat{R}_s$ ($\widehat{a}_{13}$ to $\widehat{a}_{15}$), which is computed using equation (4.2). It can be observed that in equation (4.2), the current plays an important role, hence $\widehat{R}_s$ is computed using different currents, and then an average value is obtained using the curve fitting method. The plots are shown in Figure 22. This concludes the estimation process

Table 6: Values of parameters $\widehat{a}_{13}$ to $\widehat{a}_{15}$ (simulation)

Parameter	$\widehat{a}_{13}$	$\widehat{a}_{14}$	$\widehat{a}_{15}$
Desired Value	0.1562	24.37	0.07446
Estimated Value	0.4963	33.07	0.06546
Estimation Error	2.17	35.6	0.06546

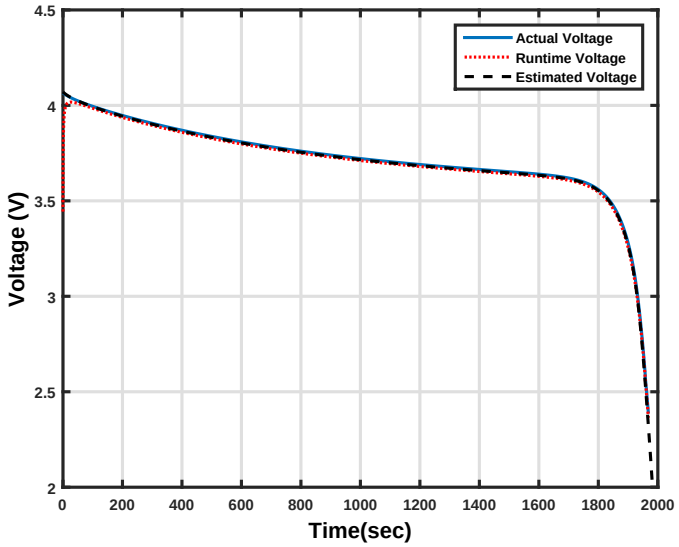

Figure 23: Actual battery vs output response with estimated parameters with respect to time (simulation results for constant discharge).

as now all the parameters are extracted. The obtained parameters along-with their respective initial conditions and bounds are presented in Table 7, whereas the parameters $\widehat{a}_{13}$ to $\widehat{a}_{15}$ are presented in Table 6. The parameters are shown in two different tables, for ease of understanding, as parameters $\widehat{a}_1$ to $\widehat{a}_{12}$ are estimated using our proposed estimation technique, whereas parameters $\widehat{a}_{13}$ to $\widehat{a}_{15}$ are calculated using the estimated values of $\widehat{a}_1$ to $\widehat{a}_{12}$. The absolute estimation error in components $\widehat{R}_{tl}$, $\widehat{C}_{tl}$, $\widehat{R}_{ts}$, $\widehat{C}_{ts}$ and the product $\widehat{R}_{tl}\widehat{C}_{tl}$ and $\widehat{R}_{ts}\widehat{C}_{ts}$ is shown in Table 7. Once the parameters are extracted, the estimated model with estimated parameters needs to be compared with the model with original parameters from [11]. A 4V and 0.275mA battery was used in the simulation as the original model [11] is available only for this rating. The estimation needs to be validated by comparison to the original model. The plots shown in Figure 23 are

Table 7: Estimation error for components $\widehat{R}_{tl}$, $\widehat{C}_{tl}$, $\widehat{R}_{ts}$, $\widehat{C}_{ts}$ (simulation)

Component	Absolute Average Estimation Error (%)
$\widehat{R}_{ts}$	8.61
$\widehat{R}_{tl}$	3.54
$\widehat{C}_{tl}$	1.326
$\widehat{C}_{ts}$	19.166
$\widehat{R}_{ts}\widehat{C}_{ts}$	1.9225
$\widehat{R}_{tl}\widehat{C}_{tl}$	0.0384

presented to validate the extracted model against the original model from [11]. Note that there are three plots in Figure 23, the runtime voltage represents the voltage curve obtained while the parameter estimation is being performed in real time, whereas the estimated voltage is obtained after the simulation is completed and the parameters are extracted, which are used in the battery model. The comparison shows that both the actual voltage and the estimated voltage match hence the battery parameter estimation is satisfactory. The Simulink models used in this work are presented in Appendix A.

Chapter 5: Experimental Validation

The experimental results of proposed adaptive parameter estimation on real Li-ion batteries are presented in this section. The results are verified by discharging the batteries using constant load at various fixed magnitudes, step discharge currents with constant step magnitudes, and step discharge currents with variable step magnitudes. This chapter is further subdivided into two sections: Section 5.1 describes the setup used to conduct real life experiments, and Section 5.2 presents the results.

5.1. Experimental Setup

The block diagram of the experimental setup is shown in Figure 24. The Li-ion battery is connected to a load through a current and voltage sensor for the voltage and current measurements. The dSpace DS 1104 control board is used to acquire the data. The experimental test bench is shown in Figure 25. A Thunder Power ($TP6600-6SP+25$) Li-ion battery rated at 22.2V, 6.6 Ah is connected with $PF2200$ series power thin film resistors, which are used as a load. Two $25\Omega, 50W$ resistors are used as individual, series and parallel combinations to construct the loads of $25\Omega, 50\Omega$, and 12.5Ω, respectively. Also, two $50W, 12V$ DC bulbs are used for rigorous load testing. Both the load current and the battery terminal voltage are monitored using a carefully calibrated LEM USA Inc LA 25-NP sensor and a 0-25V Arduino voltage sensor, respectively. The load is changed by manually inserting or removing resistors with different ratings to get the desired battery discharge currents. In order to maintain the constant operating temperature for the load resistors, a heavy duty electrical fan (i.e.,

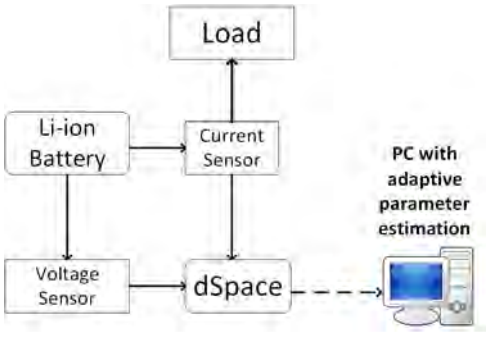

Figure 24: Block diagram for experimental setup

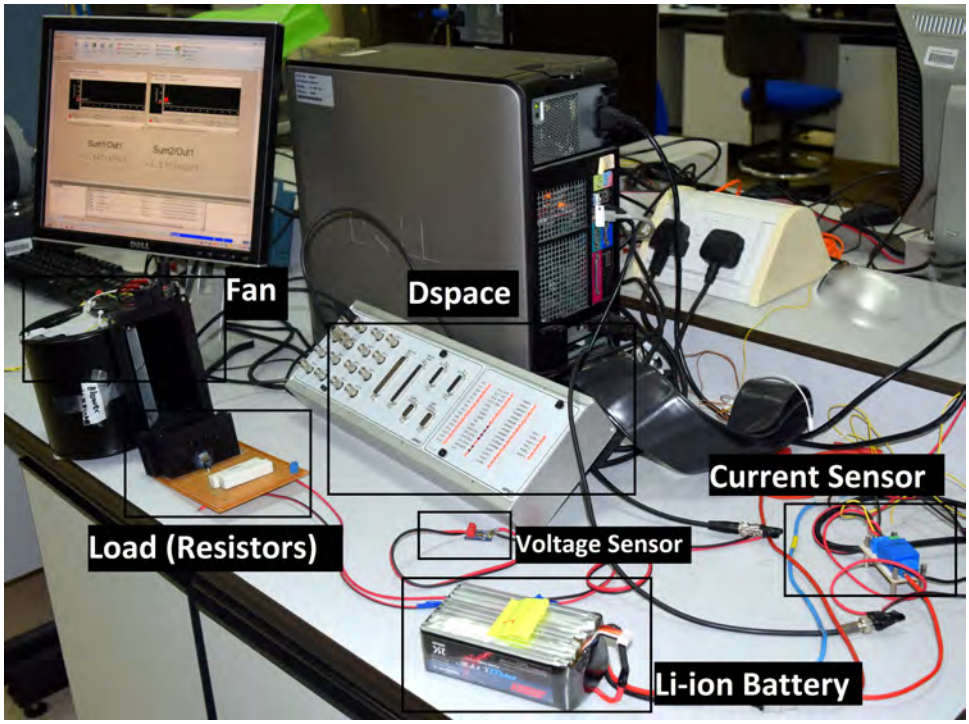

Figure 25: Test bench for adaptive battery modeling experiments

$2GDSu15-120x126L$) is used. This also helps in creating a safer work environment, as it was observed that the temperature of the power resistors can reach above 50°C. The use of the fan gives more accurate results for the current and voltage curves as the resistance of the load doesn't change much with time due to cooling provided by the fan.

5.2. Experimental Results

In this section the proposed adaptive battery parameter estimation methodology is verified through experimental results. Note that the adaptive technique can be implemented online as the battery discharges in real time, or offline as well by collecting and saving the data for later use. The battery voltage and current data have been collected through longer experimental runs which last about 4 to 16 hours. This results in an extensive amount of data, which has been observed to limit the available computer memory while running the adaptive methodology online. Therefore, the adaptive battery parameter estimation has been performed offline. The sampling frequency of the experiment is set at 100 Hz.

The experimental results are presented in the same order of conducting the tests. The steps of the estimation are already explained in Figure 18 presented in Section 4.

5.2.1. Voltage relaxation tests. The no-load EMF curve of the above battery required for estimating parameters $\widehat{a}_{16}$ to $\widehat{a}_{21}$ is obtained using the voltage relaxation method. A voltage relaxation test is performed where each cycle consists of a 15 min battery discharge stage followed by a 15 min rest stage to allow depolarization of the battery [41]. The discharge and rest cycles are repeated until the battery is completely

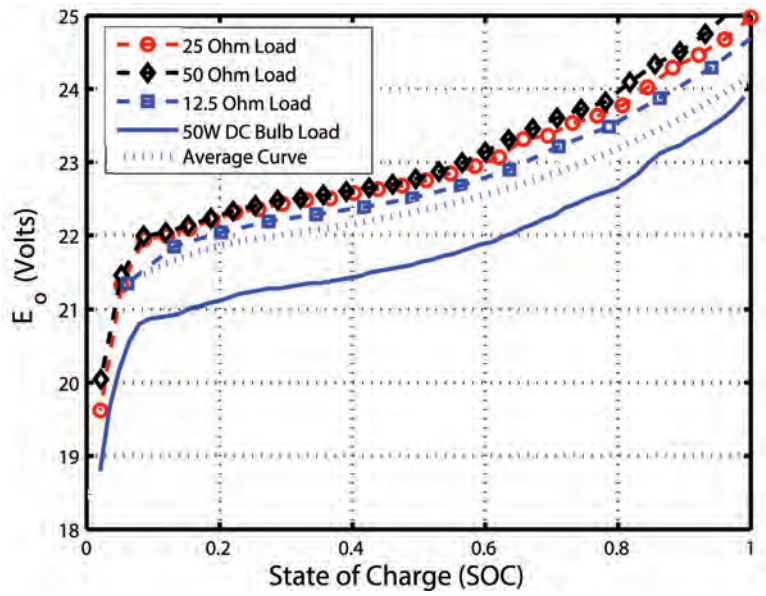

Figure 26: E_o vs SOC for different discharge currents (experimental results)

discharged. Four individual runs are performed to obtain average values of parameters $\widehat{a}_{16}$ to $\widehat{a}_{21}$. The voltage relaxation tests are conducted at different loads (25Ω, 50Ω, 12.5Ω and 50W DC Bulb) which correspond to average value of currents (860mA, 416 mA, 1741 mA and 3652 mA).

The curves presented in Figure 26 are obtained using the voltage relaxation method for the above mentioned load currents. The current plots for different loads are

Table 8: Values of estimated parameters $\widehat{a}_{16}$ to $\widehat{a}_{21}$ from experimental results

Parameter	$\widehat{a}_{16}$	$\widehat{a}_{17}$	$\widehat{a}_{18}$	$\widehat{a}_{19}$	$\widehat{a}_{20}$	$\widehat{a}_{21}$
Value	5.112	40.955	22.195	1.9215	1.7590	3.0435

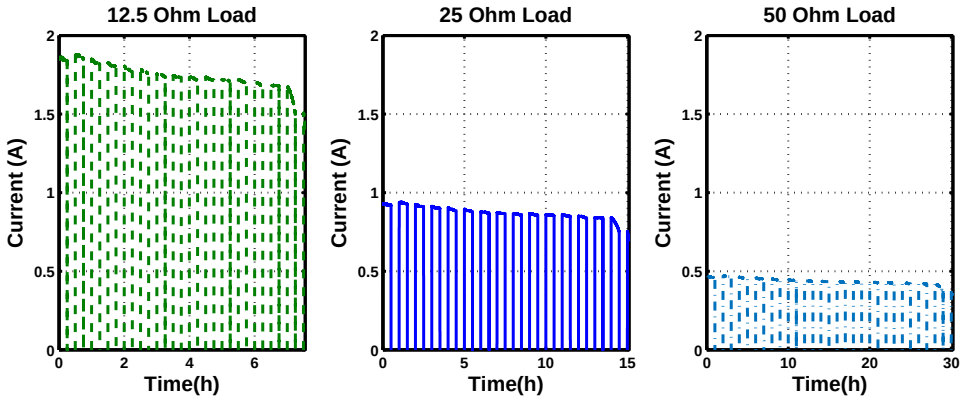

Figure 27: Current discharge curve for different loads during no load voltage relaxation tests for E_0 (experimental results)

presented in Figure 27 The relaxation time is selected to be fifteen minutes when doing the voltage relaxation experiments. For each of the above four experiments, four sets of data are obtained (i.e., four curves $\widehat{E}_0$ vs *SOC* as shown in Figure 26). For each $\widehat{E}_0$ vs *SOC* curve, the parameters $\widehat{a}_{16}$ to $\widehat{a}_{21}$ are calculated by fitting equation (2.10) to the collected data. The set of parameters obtained are named as follows: $\{\widehat{a}_{16_1},\cdots,\widehat{a}_{21_1}\}$ corresponding to 25Ω load. Similarly, $\{\widehat{a}_{16_2},\cdots,\widehat{a}_{21_2}\}$, $\{\widehat{a}_{16_3},\cdots,\widehat{a}_{21_3}\}$, $\{\widehat{a}_{16_4},\cdots,\widehat{a}_{21_4}\}$ are the parameters corresponding to loads of 50Ω, 12.5Ω and 50W DC Bulb, respectively. To attain an accurate value of the estimated parameters over the entire range of possible battery discharge currents, the parameters $\widehat{a}_{16}$ to $\widehat{a}_{21}$ are shown in Table 8, and are computed as follows:

$$\widehat{a}_{16} = \frac{1}{4}\sum_{i=1}^{4}\widehat{a}_{16_i} \tag{5.1}$$

$$\vdots$$

$$\widehat{a}_{21} = \frac{1}{4}\sum_{i=1}^{4}\widehat{a}_{21_i} \tag{5.2}$$

5.2.2. Adaptive battery parameter estimation. The battery terminal voltage data corresponding to 50Ω as load, is used to estimate the battery parameters using the adaptive parameter estimation methodology proposed in Section 4. This value of current is used because the proof explained in 4 requires minimum current to estimate

the parameters. Based upon the available loads, the minimum average current is 416mA and hence this is selected to estimate the parameters. As shown in Section 4.1.1, the estimation technique is used to get parameters $\widehat{a}_1$ to $\widehat{a}_{12}$, whereas parameters $\widehat{a}_{13}$ to $\widehat{a}_{15}$ will be obtained at the end using a separate calculation method. Further, $\widehat{a}_{16}$ to $\widehat{a}_{21}$ are already obtained from curve fitting as discussed in Section 5.2.1. For the parameters $\widehat{a}_1$ to $\widehat{a}_{12}$, the conditions mentioned in 4.1.1 are followed. Figure 28 shows the intersection of $\widehat{a}_8$ and $\widehat{a}_{11}$ with their corresponding conditions respectively. Hence, now the vertical lines can be plotted indicating the stopping stability conditions for the experimental case. The plots for $\widehat{R}_{tl}\widehat{C}_{tl}$ and $\widehat{R}_{ts}\widehat{C}_{ts}$ are shown in Figure 29. The individual plots for $\widehat{R}_{tl}$, $\widehat{R}_{ts}$, $\widehat{C}_{tl}$, and $\widehat{C}_{ts}$ are shown in Figure 30. The values of parameters $\widehat{a}_{13}$ to $\widehat{a}_{15}$ are presented in Table 9, whereas the rest of the parameters $\widehat{a}_1$ to $\widehat{a}_{12}$ are presented in Table 10. Note that the initial values used in Table 10 are far away, but the parameters still show convergence as proved in Lemma 4.1.1. This further shows that the proposed estimation technique doesn't depend on initial conditions.

5.2.3. Parameters for Rs. Once the parameters $\widehat{a}_1$ to $\widehat{a}_{12}$ are estimated, and the parameters $\widehat{a}_{16}$ to $\widehat{a}_{21}$ are extracted using the relaxation tests, the parameters for $\widehat{R}_s$

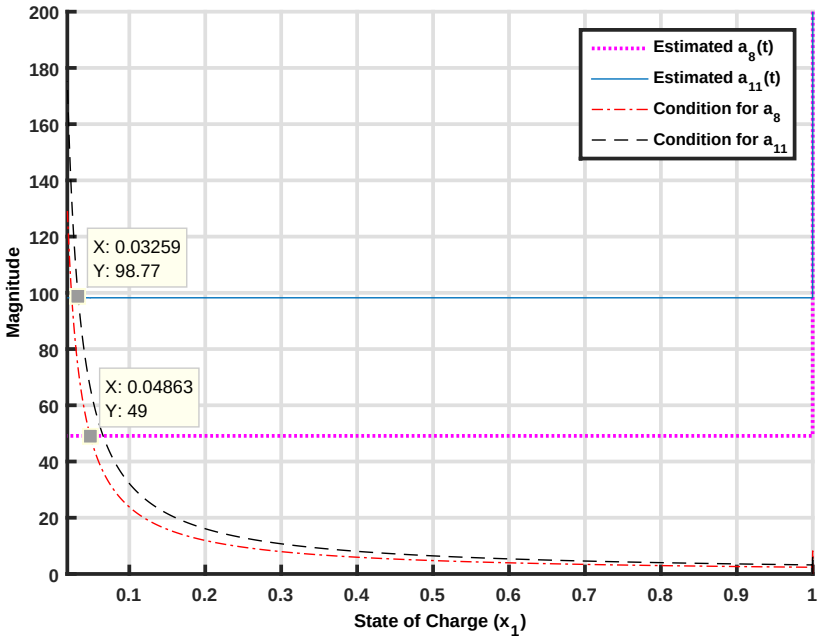

Figure 28: Intersection point of $\widehat{a}_8$ and $\widehat{a}_{11}$ with their respective stability conditions.

can be calculated using equation (4.2). The plot of $\widehat{R}_s$ using different currents is shown in Figure 31. The average value is also plotted in Figure 31. The parameters $\widehat{a}_{13}$ to $\widehat{a}_{15}$ are extracted using curve fitting on the calculated average Rs value and are presented in Table 9.

5.3. Model Validation Under Variable Load Conditions

The battery model parameters obtained by estimation technique for a load current corresponding to 50Ω load, are given in Table 10. The obtained model is rigor-

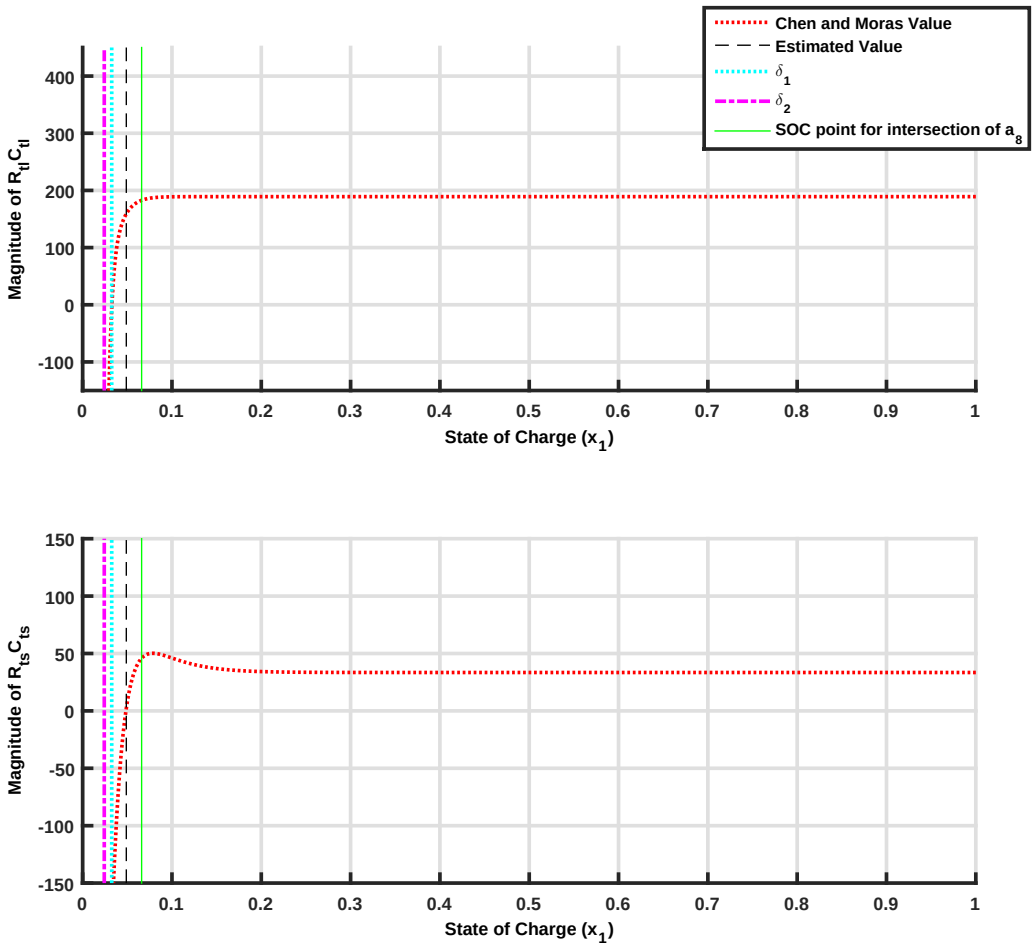

Figure 29: $\widehat{R}_{ts}\widehat{C}_{ts}$ and $\widehat{R}_{tl}\widehat{C}_{tl}$ plots of estimated parameters versus Chen and Mora's parameters (experimental results)

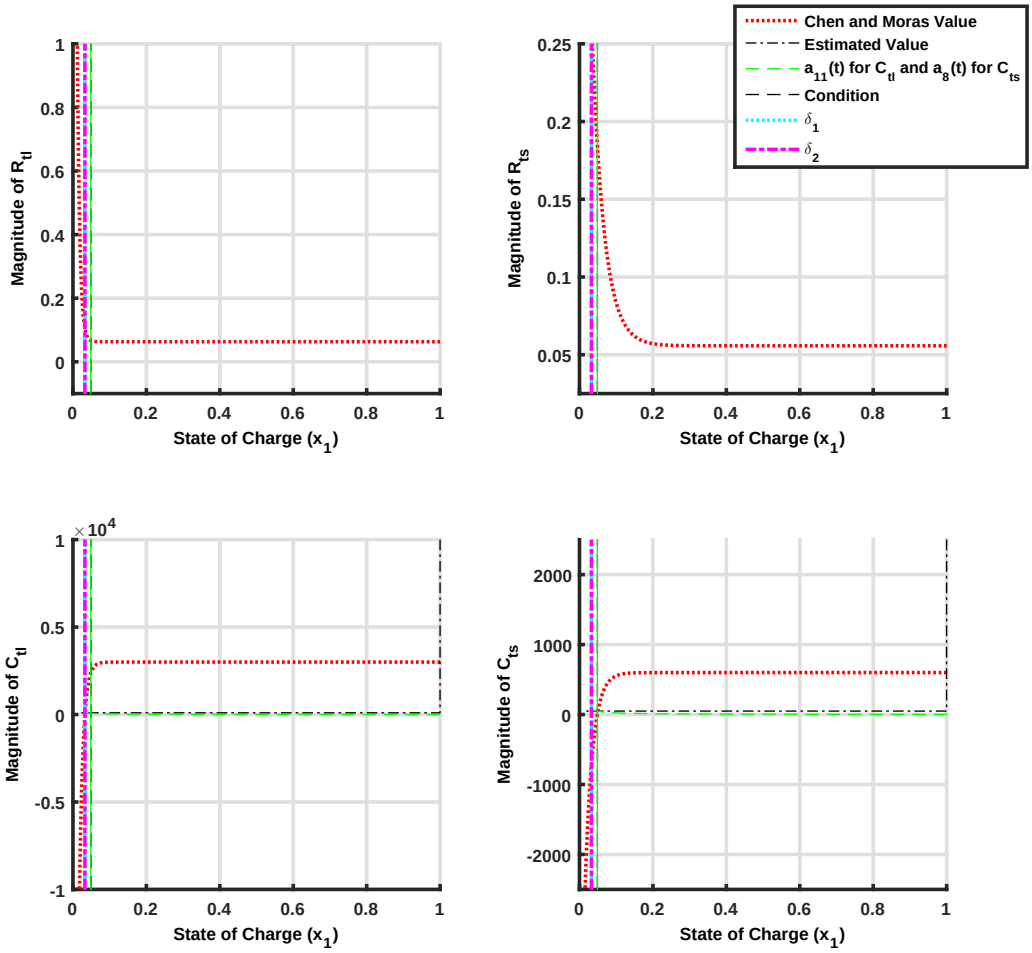

Figure 30: (Top Left) Plot for $\widehat{R}_{tl}$ with stability conditions (experimental result). (Top Right) Plot for $\widehat{R}_{ts}$ with stability conditions (experimental result). (Bottom Left) Plot for $\widehat{C}_{tl}$ with stability conditions (experimental result). (Bottom Right)Plot for $\widehat{C}_{ts}$ with stability conditions (experimental result).

ously tested by defining the following testing protocols, until the battery is completely discharged.

1. Constant loads of 50Ω, 25Ω and 12.5Ω using power resistors.
2. Constant load of 50W using DC bulbs.

Table 9: Values of parameters $\widehat{a}_{13}$ to $\widehat{a}_{15}$

Parameter	$\widehat{a}_{13}$	$\widehat{a}_{14}$	$\widehat{a}_{15}$
Experimental Value	0.0439	59.07	0.2246

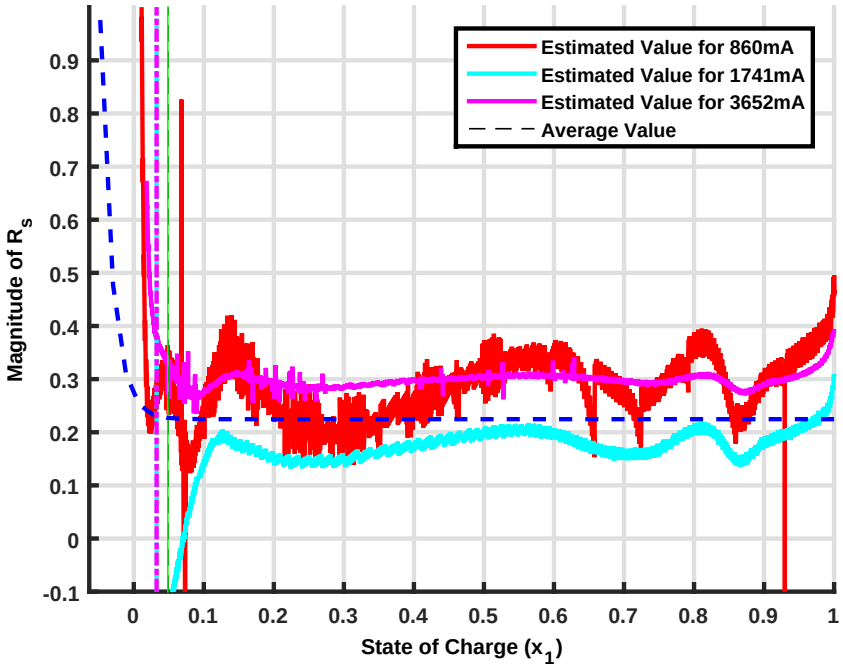

Figure 31: Calculated $\widehat{R}_s$ values for different currents

3. With a pulse discharge having no load for 15 mins and a load of 12.5Ω for 15 mins.
4. With a pulse discharge of variable loads.

Table 10: Experimental results for estimated parameters

Parameter	*Upper Bound*(a_{iu})	*Lower Bound*(a_{il})	λ_{x_i}	λ_{y_i}	*Initial Value*	*Estimated Value*
$\widehat{a}_1$	1	0.1	50	50	1800	0.5505
$\widehat{a}_2$	50	10	50	50	174000	30.0475
$\widehat{a}_3$	0.1	0.01	50	50	240	0.0551
$\widehat{a}_4$	10	1	50	50	36000	6.2585
$\widehat{a}_5$	200	100	50	50	9300	30
$\widehat{a}_6$	0.1	0.01	50	50	264	0.0551
$\widehat{a}_7$	1000	500	60	55	4512000	760.2266
$\widehat{a}_8$	30	1	50	10	78000	10.7686
$\widehat{a}_9$	800	500	80	50	5100000	685.7457
$\widehat{a}_{10}$	7000	5000	10	10	36300000	6036.4
$\widehat{a}_{11}$	50	5	50	50	162000	27.5422
$\widehat{a}_{12}$	5000	3000	10	20	42000000	3696

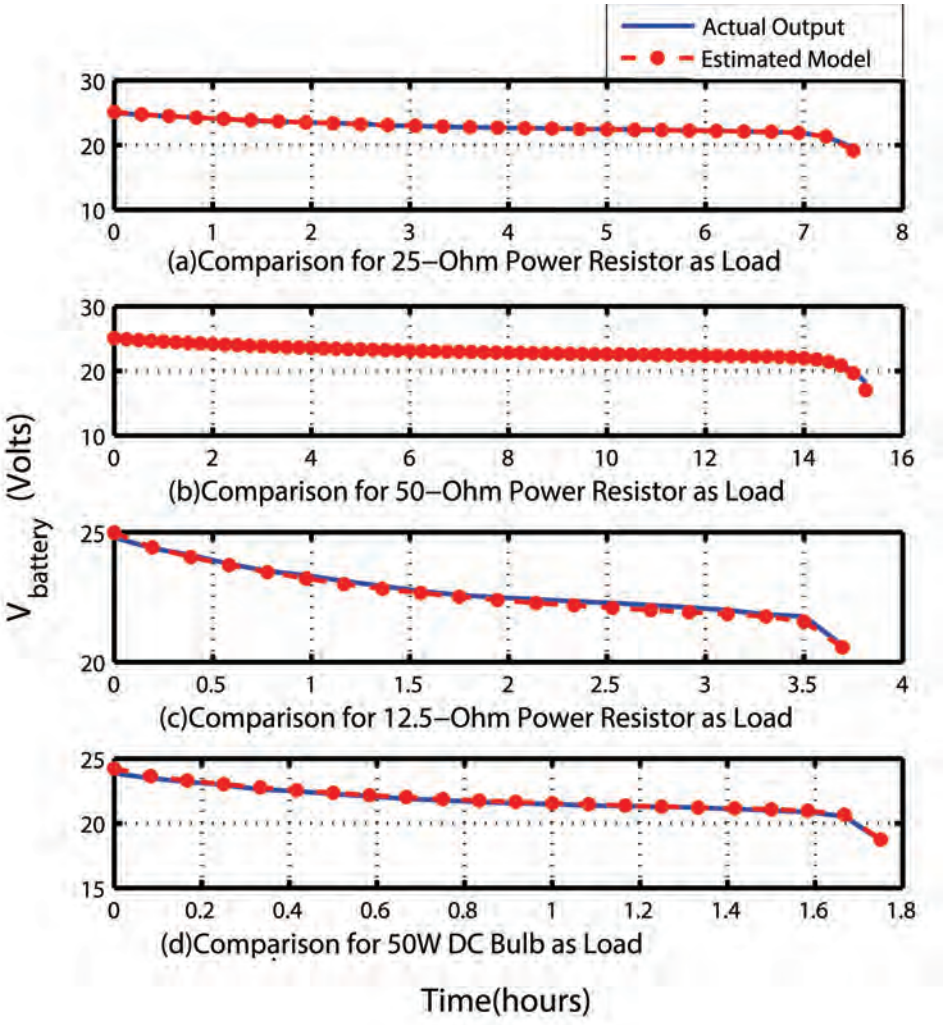

Figure 32: (a) Actual model vs estimated model comparison for 25Ω load (b) Actual model vs estimated model comparison for 50Ω load (c) Actual model vs estimated model comparison for 12.5Ω load (d) Actual model vs estimated model comparison for 50W DC bulb as load.

It is worth mentioning that for all these tests, the battery model parameters $\widehat{a}_1$ to $\widehat{a}_{12}$ are kept the same as in Table 10 i.e. parameters as estimated with a load current of 50Ω to test their insensitivity to any load change. Also, parameters $\widehat{a}_{16}$ to $\widehat{a}_{21}$ are kept the same as in Table 8. And parameters $\widehat{a}_{13}$ to $\widehat{a}_{15}$ are kept the same as in Table 9.

5.3.1. Model testing for test protocol 1 and 2. The experimental results for the constant loads are shown in Figure 32. The subplots (a), (b) and (c) show the terminal voltage curves corresponding to 25Ω load, 50Ω load and 12.5Ω load, using the power resistors. The subplot (d) shows the curve for 50W DC blub as a load. The

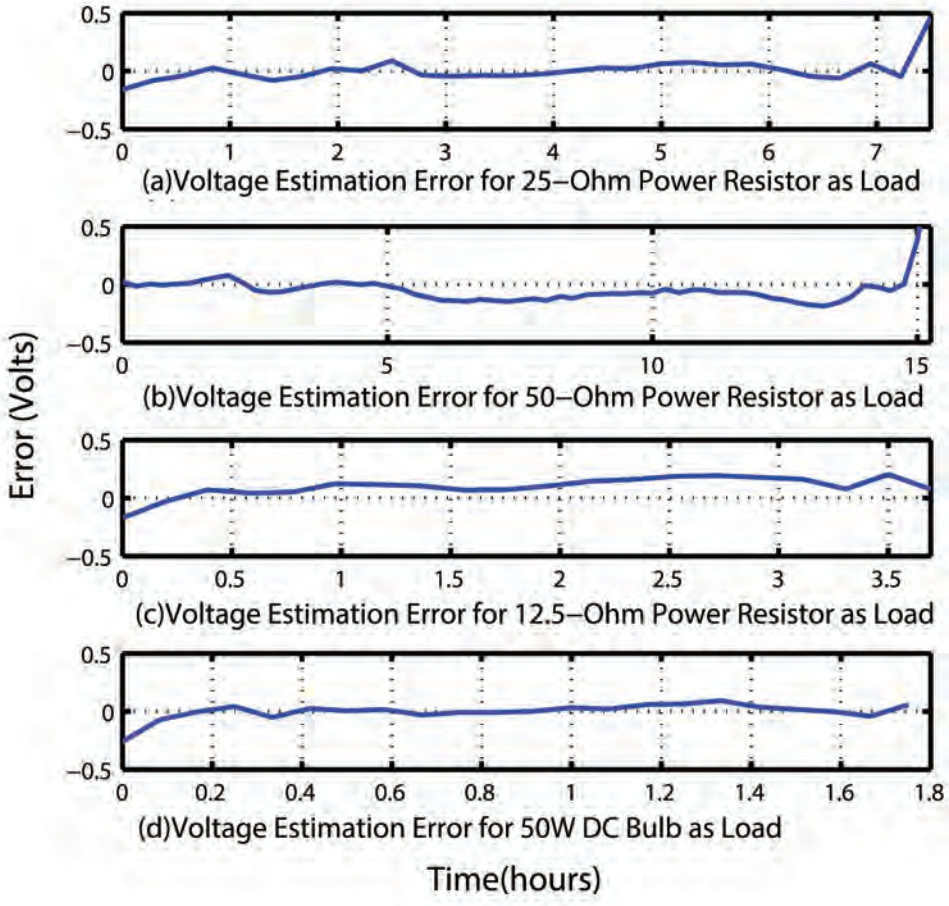

Figure 33: (a) Estimation error for 25Ω load(b) Estimation error for 50Ω load(c) Estimation error for 12.5Ω load (d) Estimation error for 50W DC bulb as load.

subplots (a) to (d) in Figure 32 show that actual battery output voltage and the estimated model's output voltage overlap with each other. The estimation error is negligibly small for these constant discharge currents as presented in Figure 33. The load currents plots are presented in Figure 34. The maximum magnitude of the error is 0.9%. These tests validate that the designed battery model is independent of the magnitude and the type of load.

5.3.2. Model testing for test protocol 3 and 4. The battery is discharged according to testing protocol 3 (i.e., with a pulse discharge having no load for 15 mins and a load of 12.5Ω for 15 mins.), and the results are presented in Figure 35. The obtained curve is then compared with the output voltage curve of the estimated model. The plots for load currents are shown in Figure 36. The maximum magnitude of the error is 0.8%. Note that the model was obtained by running the adaptive parameter

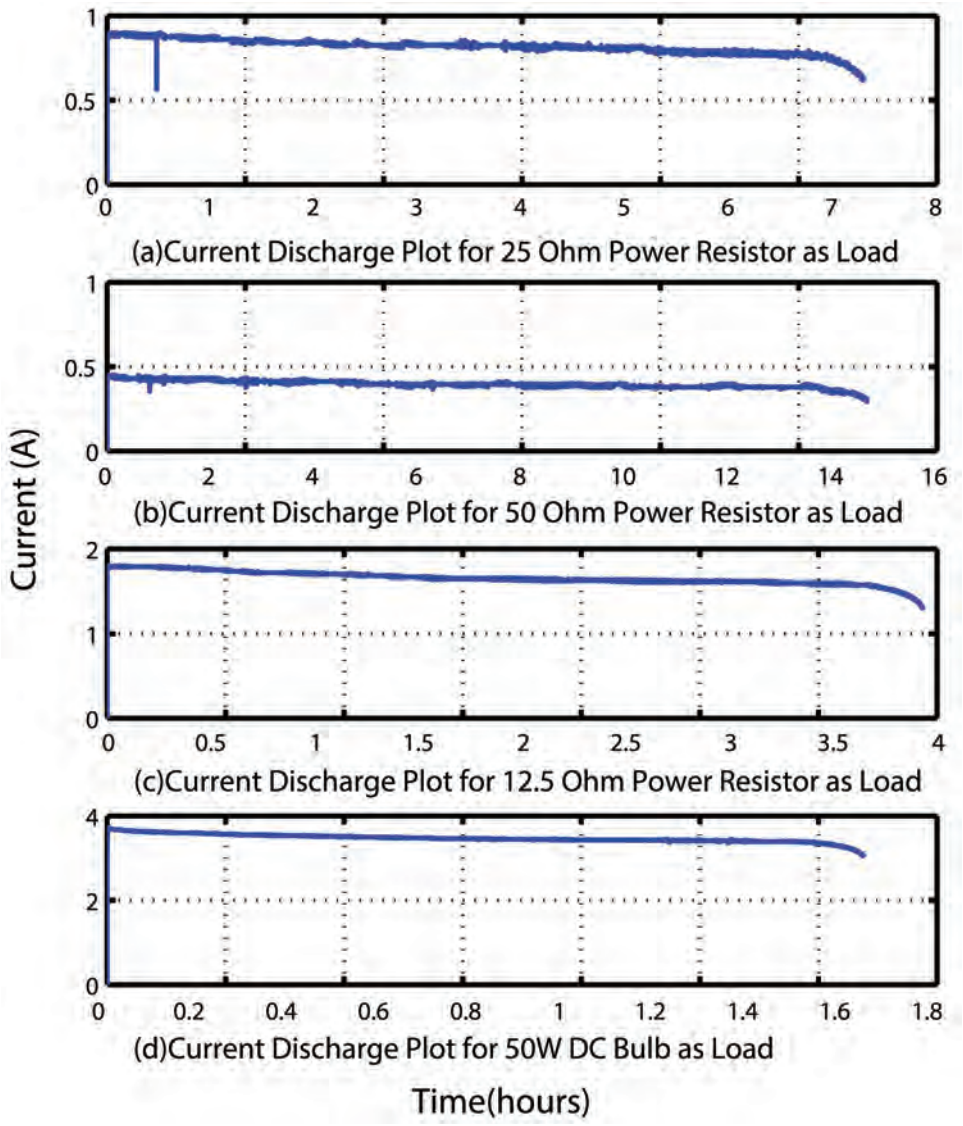

Figure 34: (a) Load current plot for discharge using 25Ω as load (b) Load current plot for discharge using 50Ω as load (c) Load current plot for discharge using 12.5Ω as load(d) Load current plot for discharge using 50W DC bulb as a load.

estimation method with a constant load of 50Ω, yet it is effectively able to estimate the output voltage accurately under the loading condition of testing protocol 3. Testing protocol 4 has a variable step discharge, in contrast to testing protocol 3, for rigorous testing of the estimated model. The experiment is started with a load of 12.5Ω. The load is increased to a 50W DC bulb and then decreased again to 12.5Ω with variable time intervals. The results for actual and estimated voltage are plotted in Figure 37. The magnitude of the error $e(t)$ is presented in Figure 38 for both constant step discharge and variable step discharge, and it shows that the estimated voltage and the actual battery

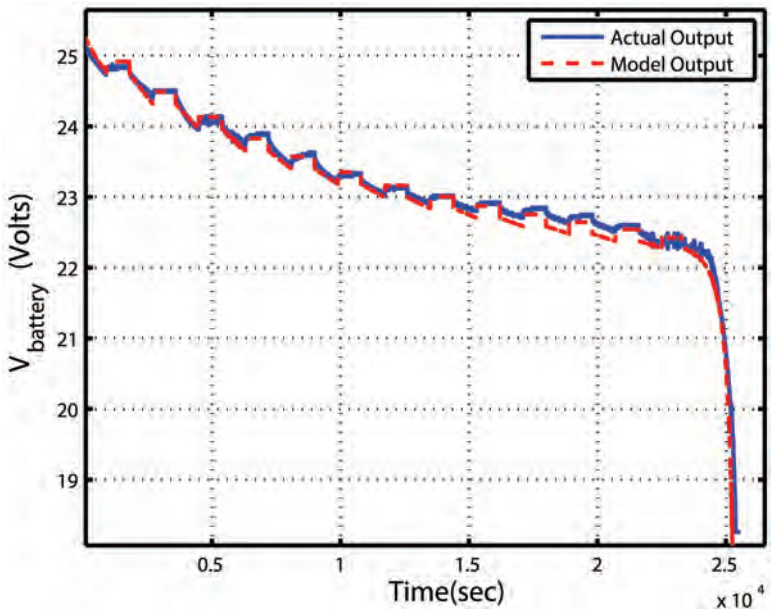

Figure 35: Actual battery vs output response with estimated parameters with respect to time (experimental results for constant step discharge)

discharge voltage are close to each other. The maximum value of the estimation error $e(t)$ is 1.5%, whereas most of the time it is close to 0.1% as observed in Figure 38. It is observed that the battery model gives an accurate estimate of the battery output voltage even under the variable magnitude square wave discharge. Hence all these

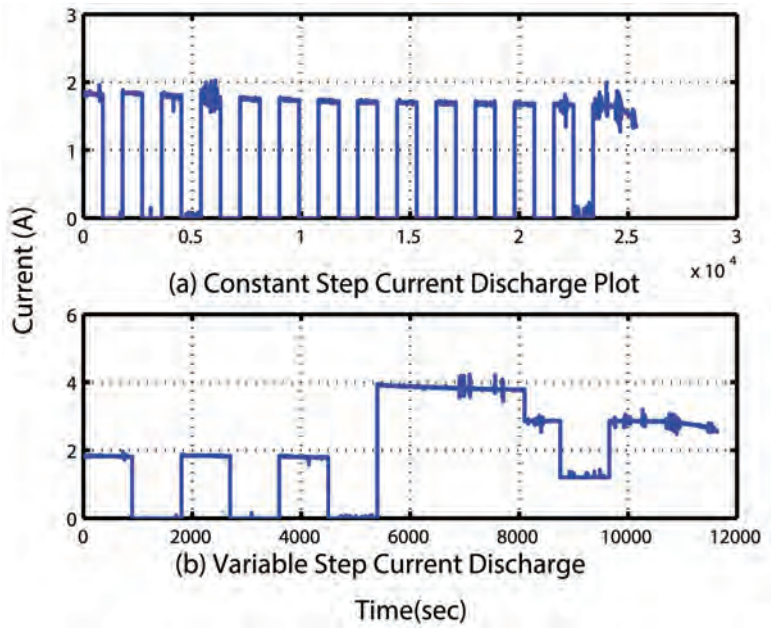

Figure 36: (a) Load current plot for constant step discharge current (b) Load current plot for variable step discharge current

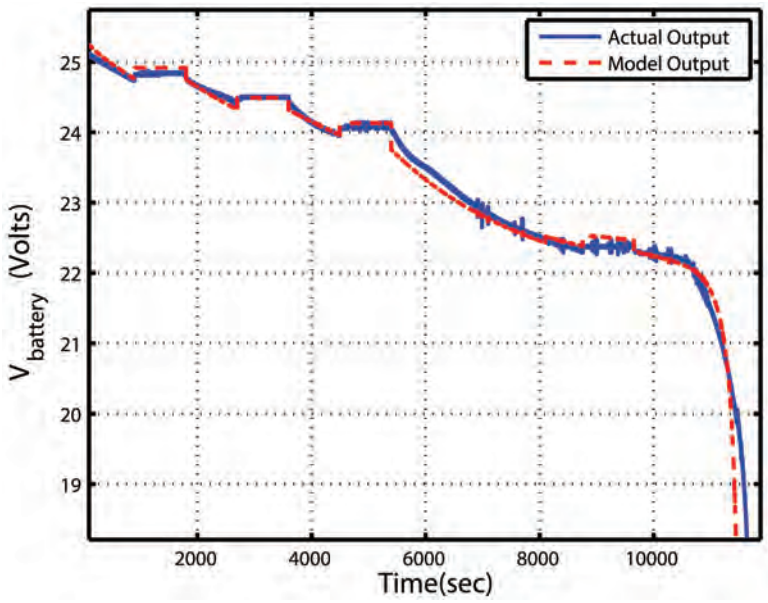

Figure 37: Actual battery vs output response with estimated parameters with respect to time (experimental results for variable step discharge)

extensive experimental results show the accuracy of the Li-ion battery model obtained by adaptive parameter estimation.

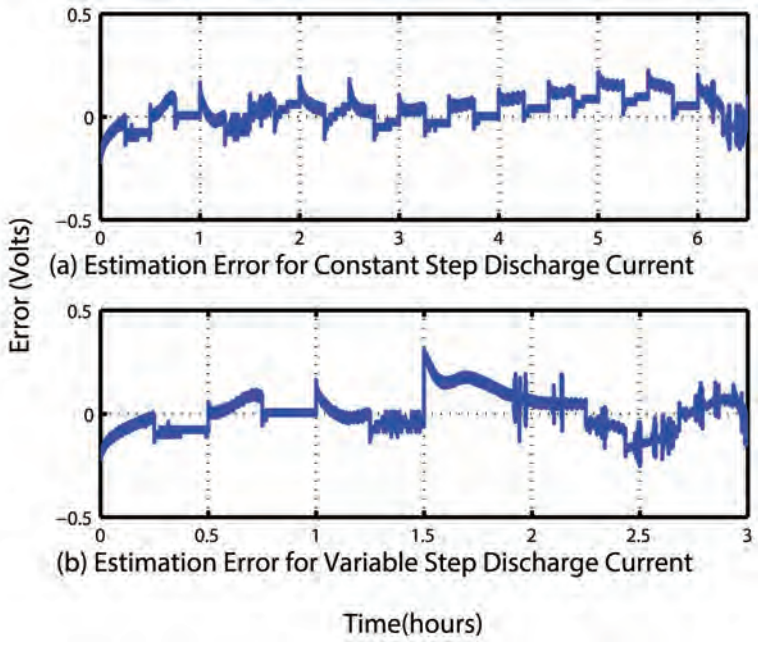

Figure 38: (a) Estimation error for constant step discharge (b) Estimation error for variable step discharge

Chapter 6: Comparative Analysis and Limitations

In this chapter, a summary of the thesis work is provided, and the limitations of the proposed battery model parameters estimation technique are discussed. The work proposes an adaptive estimation methodology to estimate the battery model parameters for Chen and Mora's model. The model used in this work, ignores the self discharging property of the batteries to simplify the model, hence our estimation technique is also not able to capture this effect. Moreover, the state of charge in this estimation technique is assumed to be the same as given by the original Chen and Mora's model, hence the state of charge is not being estimated using this modeling technique. Some improvements can be done to cover these aspects of the modeling technique to make the technique more intensive and more useful for accurate battery modeling. The es-

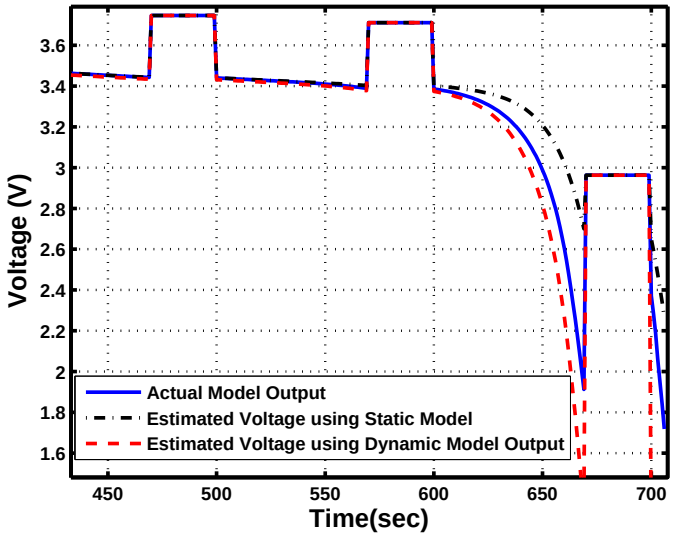

Figure 39: Dynamic model and static model with respect to time (transient response)

Table 11: Voltage estimation error for different load cases

Test Cases	Average Estimation Error for Output Voltage (%)
25Ω power resistor as constant load	0.234
50Ω power resistor as constant load	0.2697
12.5Ω power resistor as constant load	0.3390
50W DC bulb as constant load	0.1805
Constant step discharge	0.4744
Variable step discharge	0.4645

Table 12: Estimation error by using dynamic and static approaches (simulation results)

Model	Average Absolute Estimation Error for Output Voltage (%)
Estimated Dynamic Model	4.5
Estimated Static Model	6.44

timation errors between the estimated parameters $\widehat{a}_1$ to $\widehat{a}_{15}$ are shown in Table 6 and Table 7. The curves for the estimation error between the actual output and the model output are shown in Section 5 and the percentage errors are shown in Table 11. Note that despite using some assumptions in the estimation methodology, the error in the output voltage curves is very small. The methodology can be improved to reduce these errors and make the model more accurate as it is observed that the equation for $\widehat{R}_s$ gives some error in the calculation. Moreover, very small current is needed to estimate the parameters accurately so to reduce the error in the output, the current can be further reduced.

The Chen and Mora's model is a dynamic model, and this model is selected in this work so that all the dynamic characteristics i.e. no load open circuit voltage, transient response, and usable capacity of the battery can be captured. A comparison of the Chen and Mora's model with a static model is shown in Figure 39 for simulation

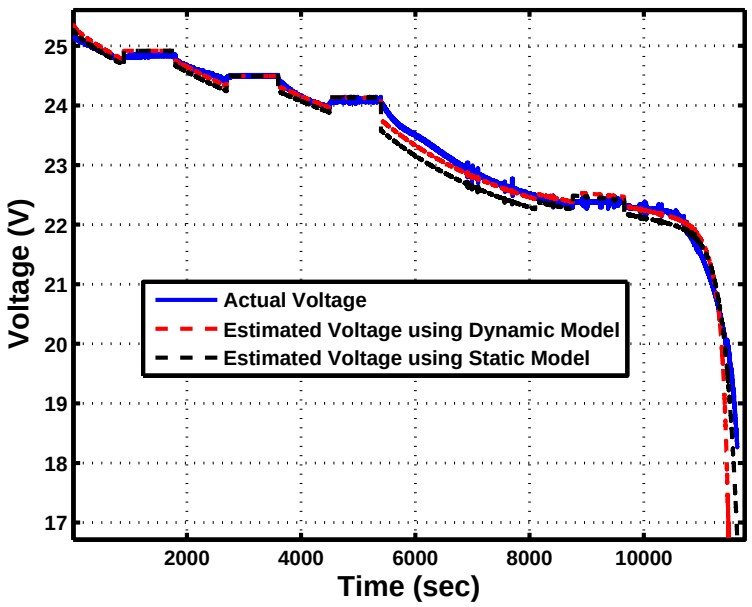

Figure 40: Actual voltage, dynamic model and static Model with respect to time. (transient response)

results. The average absolute error is presented in Table 12. The dynamic model is different than the static model in the region with low state of charge, this indicates that it is more accurate to use the state of charge x_1 in the parameters to capture all the effects of the battery model, which is the case with Chen and Mora's battery model. These results show that the dynamic model gives more accurate information about the battery. The experimental results are shown in comparison with the static and dynamic approaches in Figure 40. It can be observed that the dynamic model is more closer to the actual battery's voltage output. The average absolute error is presented in Table 13.

Table 13: Estimation error by using dynamic and static approaches (experimental results)

Model	Average Estimation Error for Output Voltage (%)
Estimated Dynamic Model	0.003
Estimated Static Model	0.358

Chapter 7: Future Work

The work done in this thesis is versatile and can be applied to the following different scenarios namely:

1. SOC Estimation.
2. Battery Fault Detection.
3. Estimating Parameters of a Fuel Cell.

The following sections provide a brief glimpse into each of the above mentioned items.

7.1. SOC Estimation

State of charge estimation can be done using the estimated battery model as follows. The E_0 curve obtained by the voltage relaxation test and the $\widehat{E}_0$ curve based on the estimated model are used in a look-up table and interpolation technique is used to extract the correct state of charge of the battery at any time instant. Note that in our parameter identification technique, coulomb counting is used to calculate the state of charge of the battery, this interpolation technique provides an alternative to extract a more accurate state of charge of the battery. The extracted state of charge is shown in Figure 41 alongwith the state of charge obtained using the coulomb counting. Note

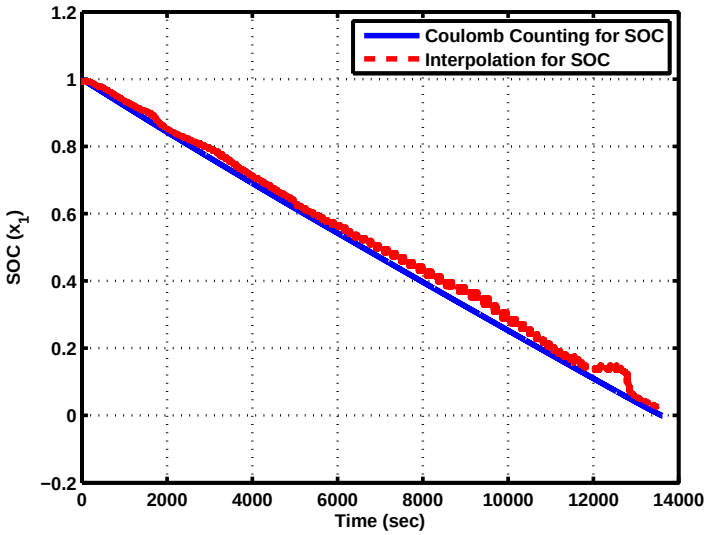

Figure 41: SOC plot for Coulomb counting vs estimated soc using constant load of 50W DC Bulb

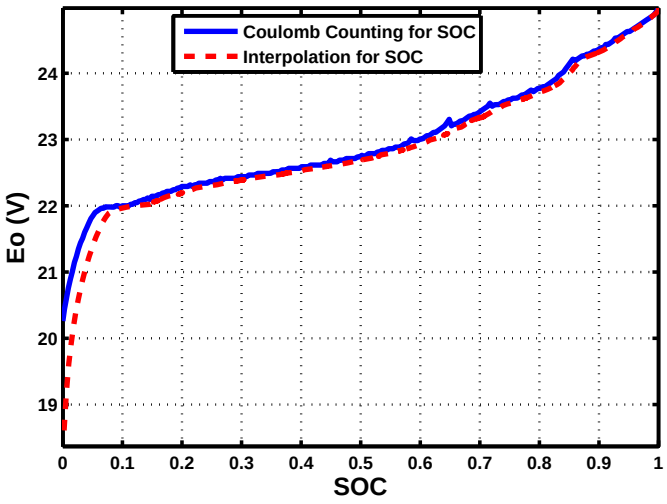

Figure 42: E_0 plot versus SOC using Coulomb counting vs estimated SOC using interpolation for constant current

that the E_0 curve for both cases is also shown in Figure 42. Hence this could lead to future work that studies and applies the state of charge estimation of a Li-ion battery using the universal adaptive stabilization technique, onto real battery energy management systems.

7.2. Battery Fault Detection

Another line of work that can be explored on the basis of the work in this thesis is battery fault detection. In most of the applications, there are battery banks comprising of huge number of batteries. If there is a faulty battery in the bank, it would keep on degrading in every cycle as the battery might be discharged more than the threshold limit. If this happens, the battery life gets damaged.

The first step is to estimate the parameters of the whole battery bank and get a model for an entire battery bank composed of many individual Li-ion batteries. Once this model is obtained, it can be used as a reference to compare the E_o curve of the bank at every cycle. If the comparison shows a difference in the state of charge of both models, it indicates that there is a faulty battery. An algorithm can be developed to sound alarm once a faulty battery is found. This can avoid catastrophic failure of an

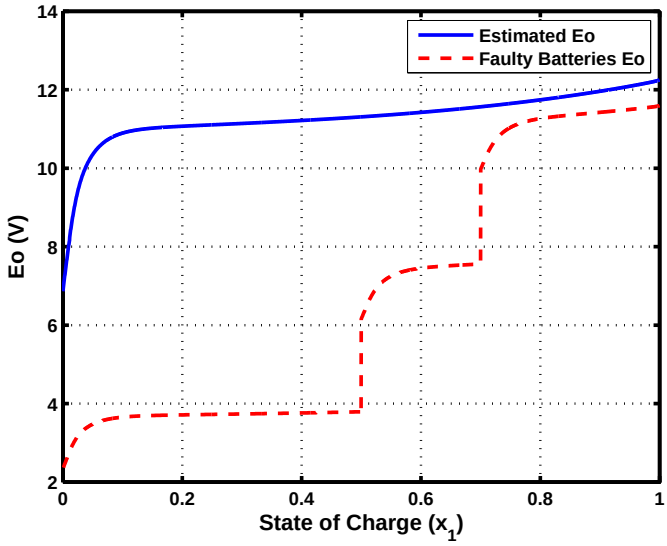

Figure 43: E_0 plot for 12V healthy battery bank versus 12V battery bank with two faulty batteries

entire battery bank due to overheating and thermal runaway caused by a single faulty battery.

The method using the E_o curve for battery fault detection is simulated for three battery banks and the result is shown in Figure 43. Note that two batteries were started at a lesser state of charge and one battery had the full state of charge. That's why the plot shows two dips corresponding to each battery's failure. An algorithm can be developed to detect the point at which these dips occur and the comparison with the estimated E_0 in a look-up table can give the correct time at which the fault occurs, and proper measures can be taken to disconnect the specific battery from the bank at that time. A future extension of this work could develop a pre-warning system which alerts

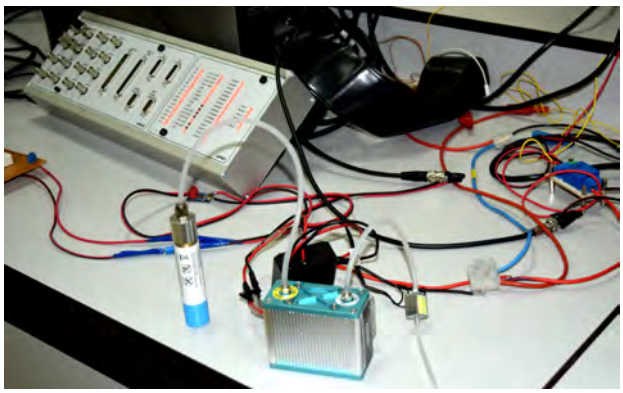

Figure 44: Experimental setup of a 30W fuel cell.

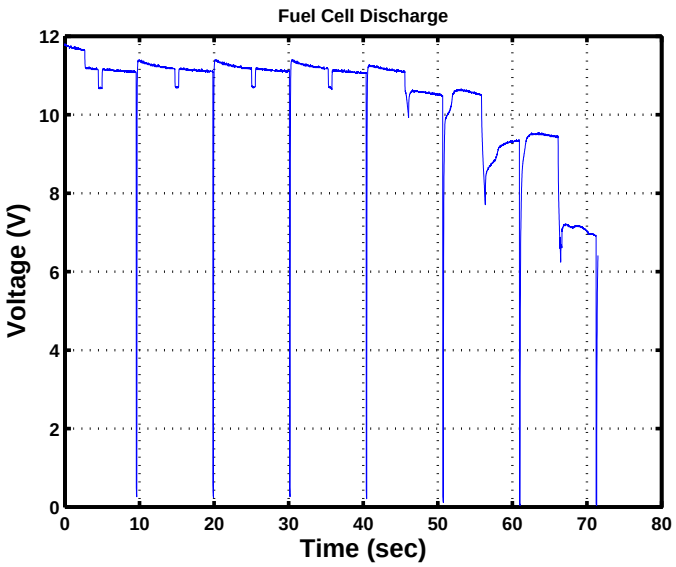

Figure 45: Voltage discharge curve of a 30W fuel cell.

a user if one of the batteries in a bank is about to fail, based only on the measurements of voltage and current at the bank level. This will therefore reduce the cost associated with installing a wiring sensor to each individual battery for detecting faults.

7.3. Estimating Model Parameters of a Fuel Cell

A small 30W fuel cell system shown in Figure 44 was used to obtain a voltage curve presented in Figure 45. The adaptive parameter estimation technique developed

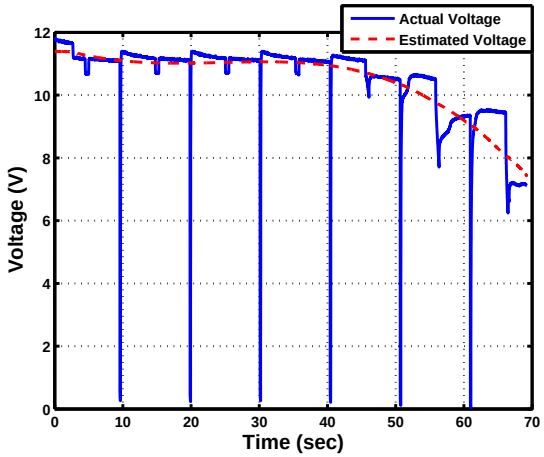

Figure 46: Voltage discharge curve versus the estimated voltage curve of a 30W fuel cell.

in this work can be applied to a given model of a fuel cell, and model parameters can be extracted. The initial results of estimation technique are shown in Figure 46. This is obtained using a simple equivalent circuit model, thus the strengths of the proposed estimation technique are obvious as it is versatile and can be applied to a variety of systems. Usually the fuel cells have very complicated models and need a lot of parameters. The modeling technique can be made less complicated by using the adaptive parameter estimation technique along with simple equivalent circuit models.

Chapter 8: Conclusion

In this work a high gain adaptive observer-based battery model parameters estimation technique is presented for Li-ion batteries. The methodology assumes that the batteries have a particular structure inspired by Chen and Mora's battery model. The Li-ion battery model requires twenty one parameters out of which six parameters corresponding to the shape of the no-load EMF curve are obtained via a voltage relaxation test and curve fitting. The remaining parameters are estimated using an adaptive parameters estimation technique. Initially three schemes are proposed for the adaptive parameter estimation of the desired parameters. Based on the observations, an improved estimation technique is proposed which requires less experimentation to estimate the battery model parameters.

The battery model parameters estimation techniques have been thoroughly simulated and experimentally validated. The experiments are done on constant loads as well as variable loads to check the accuracy of the estimated model. The estimated model performs reasonably accurately and the estimation error is very small. The mathematical proof is also presented showing the convergence of the parameters to the actual values which further validates our work. The novel contributions of this work are: (i) The development of battery model parameters estimation methodology using a universal adaptive stabilizer, which provides battery parameters that are independent of the magnitude and type of load; (ii) The proposed technique requires only a few tests to produce a sufficiently accurate model in contrast to experimental battery modeling techniques available in the literature requiring many charge/discharge tests on a battery.

References

[1] F. H. Cocks, *Energy Demand and Climate Change: Issues and Resolutions*, 1st ed. Wiley-VCH, 5 2009.

[2] C. Li, Z. Chen, J. Cui, Y. Wang, and F. Zou, "The lithium-ion battery state-of-charge estimation using random forest regression," in *2014 Prognostics and System Health Management Conference (PHM-2014 Hunan)*, Aug 2014, pp. 336–339.

[3] D. Simon, *Optimal State Estimation: Kalman, H Infinity, and Nonlinear Approaches*. John Wiley & Sons, 2006.

[4] N. A. Chaturvedi, R. Klein, J. Christensen, J. Ahmed, and A. Kojic, "Modeling, estimation, and control challenges for lithium-ion batteries," in *American Control Conference (ACC), 2010*, June 2010, pp. 1997–2002.

[5] J. Xu, B. Cao, J. Cao, Z. Zou, C. C. Mi, and Z. Chen, "A Comparison Study of the Model Based SOC Estimation Methods for Lithium-Ion Batteries," in *2013 IEEE Vehicle Power and Propulsion Conference (VPPC)*, Oct 2013, pp. 1–5.

[6] S. Kai and S. Qifang, "Overview of the types of battery models," in *2011 30th Chinese Control Conference (CCC)*, July 2011, pp. 3644–3648.

[7] M. S. Farag, R. Ahmed, S. A. Gadsden, S. R. Habibi, and J. Tjong, "A comparative study of Li-ion battery models and nonlinear dual estimation strategies," in *2012 IEEE Transportation Electrification Conference and Expo (ITEC)*, June 2012, pp. 1–8.

[8] J. Newman, K. E. Thomas, H. Hafezi, and D. R. Wheeler, "Modeling of lithium-ion batteries," *Journal of Power Sources*, vol. 119, pp. 838–843, 2003.

[9] P. Rong and M. Pedram, "An analytical model for predicting the remaining battery capacity of lithium-ion batteries," *IEEE Transactions on Very Large Scale Integration (VLSI) Systems*, vol. 14, no. 5, pp. 441–451, May 2006.

[10] D. Rakhmatov, S. Vrudhula, and D. Wallach, "A model for battery lifetime analysis for organizing applications on a pocket computer," *IEEE Transactions on Very Large Scale Integration (VLSI) Systems*, vol. 11, no. 6, pp. 1019–1030, Dec 2003.

[11] M. Chen and G. Rincon-Mora, "Accurate electrical battery model capable of predicting runtime and I-V performance," *IEEE Transactions on Energy Conversion*, vol. 21, no. 2, pp. 504–511, June 2006.

[12] L. Gao, S. Liu, and R. Dougal, "Dynamic lithium-ion battery model for system simulation," *IEEE Transactions on Components and Packaging Technologies*, vol. 25, no. 3, pp. 495–505, Sep 2002.

[13] Y.-C. Hsieh, T.-D. Lin, and R.-J. Chen, "Li-ion battery model exploring by intermittent discharging," in *2012 International Conference on Renewable Energy Research and Applications (ICRERA)*, Nov 2012, pp. 1–5.

[14] H. Rahimi-Eichi and M.-Y. Chow, "Adaptive parameter identification and State-of-Charge estimation of lithium-ion batteries," in *IECON 2012 - 38th Annual Conference on IEEE Industrial Electronics Society*, Oct 2012, pp. 4012–4017.

[15] H. Rahimi-Eichi, F. Baronti, and M.-Y. Chow, "Online Adaptive Parameter Identification and State-of-Charge Coestimation for Lithium-Polymer Battery Cells," *IEEE Transactions on Industrial Electronics*, vol. 61, no. 4, pp. 2053–2061, April 2014.

[16] H. Rahimi-Eichi, F. Baronti, and M.-Y. Chow, "Modeling and online parameter identification of Li-Polymer battery cells for SOC estimation," in *2012 IEEE International Symposium on Industrial Electronics (ISIE)*, May 2012, pp. 1336–1341.

[17] H. Chaoui, N. Golbon, I. Hmouz, R. Souissi, and S. Tahar, "Lyapunov-Based Adaptive State of Charge and State of Health Estimation for Lithium-Ion Batteries," *IEEE Transactions on Industrial Electronics*, vol. 62, no. 3, pp. 1610–1618, March 2015.

[18] D. Kapoor, P. Sodhi, and A. Keyhani, "Estimation of parameters for battery storage models," in *2014 IEEE Conference on Energy Conversion (CENCON)*, Oct 2014, pp. 406–411.

[19] R. Xiong, H. He, F. Sun, and K. Zhao, "Evaluation on State of Charge Estimation of Batteries With Adaptive Extended Kalman Filter by Experiment Approach," *IEEE Transactions on Vehicular Technology*, vol. 62, no. 1, pp. 108–117, Jan 2013.

[20] P. Kumar and P. Bauer, "Parameter extraction of battery models using multiobjective optimization genetic algorithms," in *2010 14th International Power Electronics and Motion Control Conference (EPE/PEMC)*, Sept 2010, pp. T9–106–T9–110.

[21] J. Remmlinger, M. Buchholz, and K. Dietmayer, "Identification of a bilinear and parameter-varying model for lithium-ion batteries by subspace methods," in *2013 American Control Conference (ACC)*, June 2013, pp. 2268–2273.

[22] D. Shin, M. Poncino, E. Macii, and N. Chang, "A Statistical Model-Based Cell-to-Cell Variability Management of Li-ion Battery Pack," *IEEE Transactions on Computer-Aided Design of Integrated Circuits and Systems*, vol. 34, no. 2, pp. 252–265, Feb 2015.

[23] J. V. Barreras, E. Schaltz, S. J. Andreasen, and T. Minko, "Datasheet-based modeling of li-ion batteries," in *Vehicle Power and Propulsion Conference (VPPC), 2012 IEEE*, Oct 2012, pp. 830–835.

[24] N. Nagaoka and A. Ametani, "An estimation method of Li-ion battery impedance using z-transform," in *2012 IEEE 13th Workshop on Control and Modeling for Power Electronics (COMPEL)*, June 2012, pp. 1–6.

[25] A. Mills and J. Zambreno, "Estimating state of charge and state of health of rechargable batteries on a per-cell basis," in *2015 Workshop on Modeling and Simulation of Cyber-Physical Energy Systems (MSCPES)*, April 2015, pp. 1–6.

[26] K. Mueller, E. Schwiederik, and D. Tittel, "Analysis of parameter identification methods for electrical li-ion battery modelling," in *2013 World Electric Vehicle Symposium and Exhibition (EVS27)*, Nov 2013, pp. 1–9.

[27] S. Gold, "A PSPICE macromodel for lithium-ion batteries," in *Twelfth Annual Battery Conference on Applications and Advances, 1997*, Jan 1997, pp. 215–222.

[28] H. Macicior, M. Oyarbide, O. Miguel, I. Cantero, J. M. Canales, and A. Etxeberria, "Iterative capacity estimation of LiFePO4 cell over the lifecycle based on SoC estimation correction," in *2013 World Electric Vehicle Symposium and Exhibition (EVS27)*, Nov 2013, pp. 1–10.

[29] B. Pattipati, C. Sankavaram, and K. Pattipati, "System identification and estimation framework for pivotal automotive battery management system characteristics," *IEEE Transactions on Systems, Man, and Cybernetics, Part C (Applications and Reviews)*, vol. 41, no. 6, pp. 869–884, Nov 2011.

[30] Y. Hu and Y. Y. Wang, "Two time-scaled battery model identification with application to battery state estimation," *IEEE Transactions on Control Systems Technology*, vol. 23, no. 3, pp. 1180–1188, May 2015.

[31] V. Agarwal, K. Uthaichana, R. A. DeCarlo, and L. H. Tsoukalas, "Development and validation of a battery model useful for discharging and charging power control and lifetime estimation," *IEEE Transactions on Energy Conversion*, vol. 25, no. 3, pp. 821–835, Sept 2010.

[32] P. Shi, C. Bu, and Y. Zhao, "The ANN models for SOC/BRC estimation of Li-ion battery," in *2005 IEEE International Conference on Information Acquisition*, June 2005, pp. 5 pp.–.

[33] M. F. Samadi, S. M. M. Alavi, and M. Saif, "Online state and parameter estimation of the Li-ion battery in a Bayesian framework," in *2013 American Control Conference (ACC)*, June 2013, pp. 4693–4698.

[34] Z. Zhang, "Modeling a lithium-ion battery based on a threshold model," in *2015 International Conference on Advanced Mechatronic Systems (ICAMechS)*, Aug 2015, pp. 301–305.

[35] L. Liu, L. Y. Wang, Z. Chen, C. Wang, F. Lin, and H. Wang, "Integrated system identification and state-of-charge estimation of battery systems," in *2013 IEEE Power and Energy Society General Meeting (PES)*, July 2013, pp. 1–1.

[36] L. Xintian, Z. Guojian, H. Yao, D. Bo, and X. Xingwu, "Research on the capacity fading characteristics of a Li-ion battery based on an equivalent thermal model," in *2014 International Conference on Intelligent Computing and Internet of Things (ICIT)*, Jan 2015, pp. 145–150.

[37] S. Mukhopadhyay and F. Zhang, "A high-gain adaptive observer for detecting Li-ion battery terminal voltage collapse," *Automatica*, vol. 50, no. 3, pp. 896 – 902, 2014, [accessed 19-July-2015]. [Online]. Available: http://www.sciencedirect.com/science/article/pii/S0005109813005700

[38] G. L. Plett, "Extended Kalman filtering for battery management systems of LiPB-based {HEV} battery packs: Part 1. Background," *Journal of Power Sources*, vol. 134, no. 2, pp. 252 – 261, 2004, [accessed 13-Oct-2015]. [Online]. Available: http://www.sciencedirect.com/science/article/pii/S0378775304003593

[39] V. Knap, D. I. Stroe, R. Teodorescu, M. Swierczynski, and T. Stanciu, "Electrical circuit models for performance modeling of Lithium-Sulfur batteries," in *2015 IEEE Energy Conversion Congress and Exposition (ECCE)*, Sept 2015, pp. 1375–1381.

[40] M. Knauff, C. Dafis, D. Niebur, H. Kwatny, and C. Nwankpa, "Simulink Model for Hybrid Power System Test-bed," in *ESTS '07. IEEE Electric Ship Technologies Symposium*, May 2007, pp. 421–427.

[41] M. Petzl and M. Danzer, "Advancements in OCV Measurement and Analysis for Lithium-Ion Batteries," *IEEE Transactions on Energy Conversion*, vol. 28, no. 3, pp. 675–681, Sept 2013.

[42] F. Zhang, Z. Shi, and S. Mukhopadhyay, "Robustness analysis for battery supported cyber-physical systems," *ACM Transactions on Embedded Computing Systems (TECS)*, vol. 12, no. 3, p. 69, 2013.

[43] D. H. Owens, "Universal adaptive stabilization approaches to nonlinear control," in *IEE Colloquium on Non-Linear Control*, May 1994, pp. 3/1–3/2.

[44] Y. Miyasato, "A design method of universal adaptive stabilizer," *IEEE Transactions on Automatic Control*, vol. 45, no. 12, pp. 2368–2373, Dec 2000.

[45] A. Ilchmann, "Non-identifier-based high-gain adaptive control," *Springer, New York*, 1993.

[46] *Special Functions for Applied Scientists*. New York, NY: Springer New York, 2008, ch. Mittag-Leffler Functions and Fractional Calculus, pp. 79–134. [Online]. Available: http://dx.doi.org/10.1007/978-0-387-75894-7_2

[47] Y. Li and Y. Chen, "When is a Mittag Leffler function a Nussbaum function?" *Automatica*, vol. 45, no. 8, pp. 1957 – 1959, 2009, [accessed 20-Oct-2015]. [Online]. Available: http://www.sciencedirect.com/science/article/pii/S0005109809001800

[48] S. Mukhopadhyay. (2008) Mittag-Leffler function, m-file, CMEX DLL, and s-function. [accessed 02-Jan-2016]. [Online]. Available: http://www.mathworks.com/matlabcentral/fileexchange/20731-mittag-leffler-functionm-filecmex-dlland-s-function

[49] S. Mukhopadhyay, Y. Li, and Y. Q. Chen, "Experimental Studies of a Fractional Order Universal Adaptive Stabilizer," in *2008. IEEE/ASME International Conference on Mechtronic and Embedded Systems and Applications*, Oct 2008, pp. 591–596.

[50] M. Jankovic, "Adaptive nonlinear output feedback tracking with a partial high-gain observer and backstepping," *IEEE Transactions on Automatic Control*, vol. 42, no. 1, pp. 106–113, Jan 1997.

[51] E. Bullinger and F. Allgower, "An adaptive high-gain observer for nonlinear systems," in *Proceedings of the 36th IEEE Conference on Decision and Control, 1997.*, vol. 5, Dec 1997, pp. 4348–4353 vol.5.

Appendix-A: Simulink models

The simulink models used in the proposed battery estimation technique are presented in Figures 47-49. The Mittag-Leffler function is also shown in Figure 50.

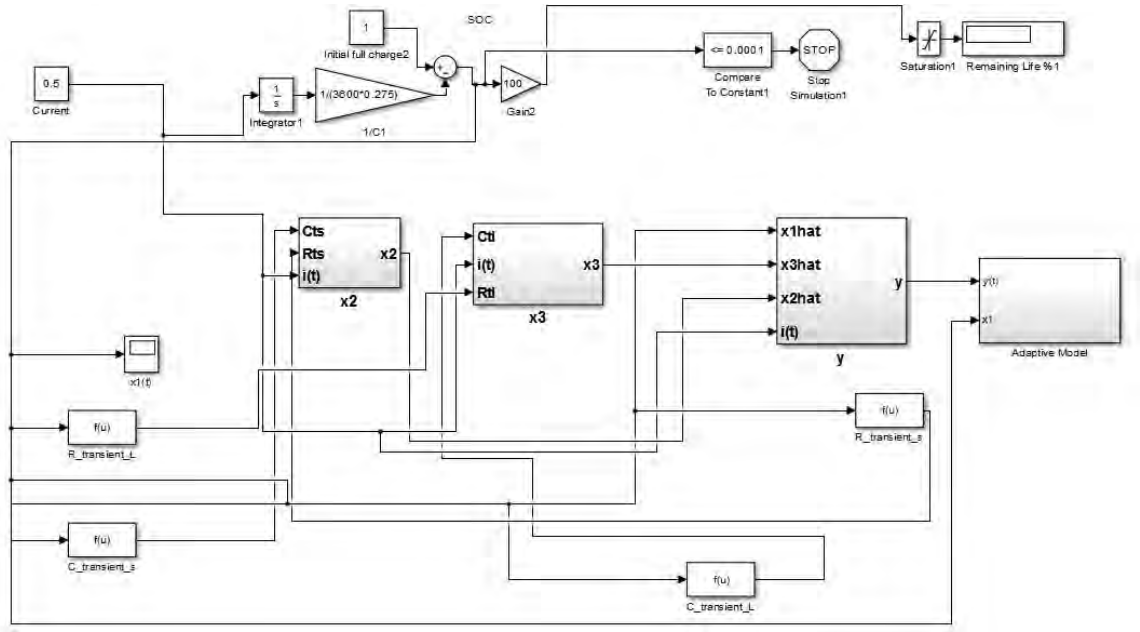

Figure 47: Simulink diagram of overall algorithm

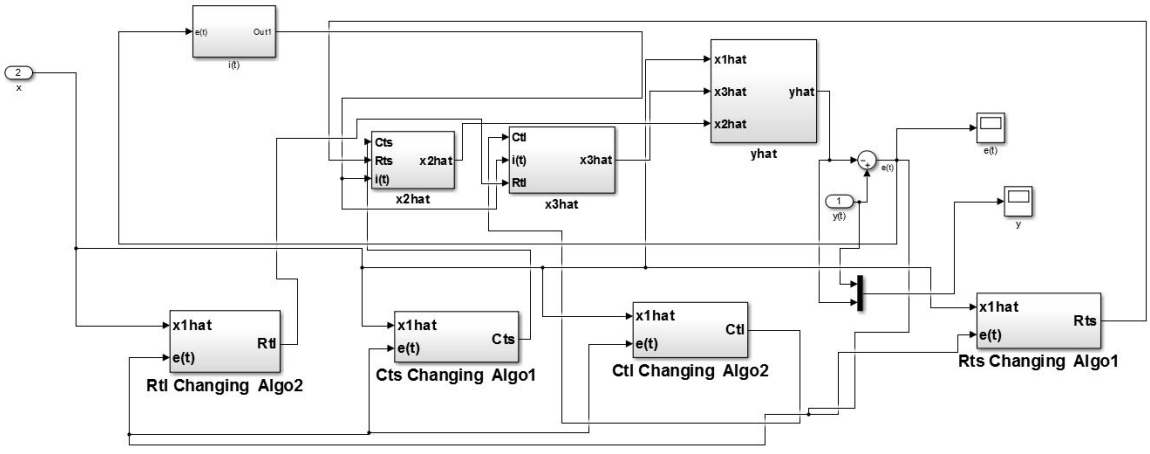

Figure 48: Adaptive model block

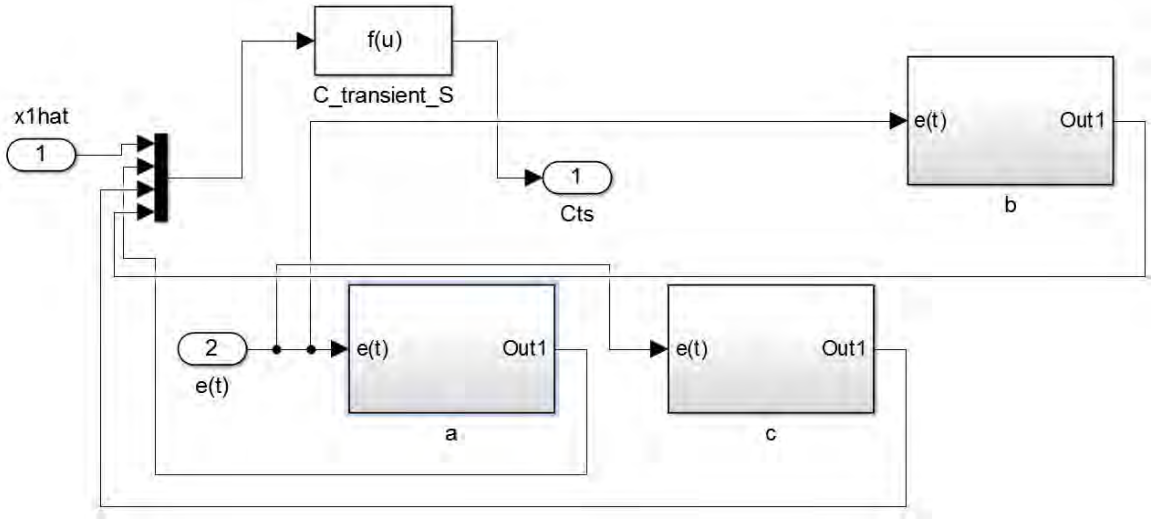

Figure 49: Cts block

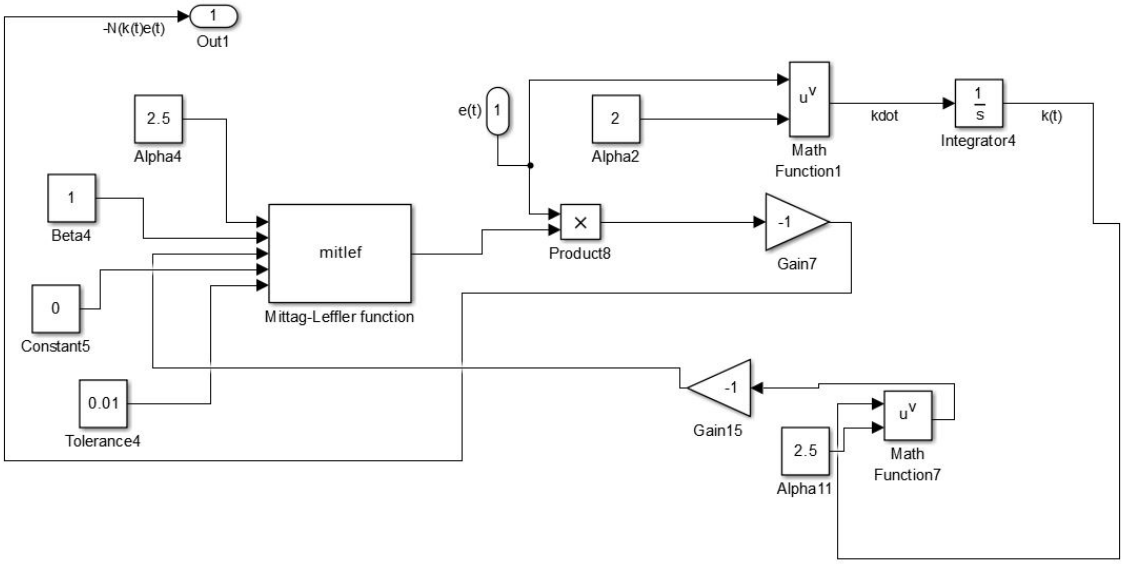

Figure 50: Mittag-Leffler function used in simulation

Vita

Daniyal Ali was born in 1990, in Gujranwala, Pakistan. He moved to Rawalpindi to complete his high school. In year 2009, he joined National University of Sciences and Technology (NUST), Islamabad, Pakistan, where he got a partial scholarship to graduate with a Bachelor of Science in Electrical Engineering in 2013. In the same year, Daniyal joined a private company in Pakistan that dealt with the Renewable Energy. He worked from August 2013 to August 2014 as a Field Engineer. Daniyal joined Masters program of Electrical Engineering at American University of Sharjah (AUS), Sharjah, UAE in 2014, where he was awarded with a graduate assistantship to pursue his studies. This gave him an opportunity to work as a teaching assistant from September 2014 until June 2016.